RSC Advances

REVIEW

View Article Online
View Journal | View Issue

Cite this: *RSC Adv.*, 2022, **12**, 12477

Recent advances in the application of parahydrogen in catalysis and biochemistry†

Gerd Buntkowsky, *[a] Franziska Theiss,[a] Jonas Lins,[a] Yuliya A. Miloslavina,[a] Laura Wienands,[a] Alexey Kiryutin[b] and Alexandra Yurkovskaya[b]

Nuclear Magnetic Resonance (NMR) spectroscopy and Magnetic Resonance Imaging (MRI) are analytical and diagnostic tools that are essential for a very broad field of applications, ranging from chemical analytics, to non-destructive testing of materials and the investigation of molecular dynamics, to *in vivo* medical diagnostics and drug research. One of the major challenges in their application to many problems is the inherent low sensitivity of magnetic resonance, which results from the small energy-differences of the nuclear spin-states. At thermal equilibrium at room temperature the normalized population difference of the spin-states, called the Boltzmann polarization, is only on the order of 10^{-5}. Parahydrogen induced polarization (PHIP) is an efficient and cost-effective hyperpolarization method, which has widespread applications in Chemistry, Physics, Biochemistry, Biophysics, and Medical Imaging. PHIP creates its signal-enhancements by means of a reversible (SABRE) or irreversible (classic PHIP) chemical reaction between the parahydrogen, a catalyst, and a substrate. Here, we first give a short overview about parahydrogen-based hyperpolarization techniques and then review the current literature on method developments and applications of various flavors of the PHIP experiment.

Received 28th February 2022
Accepted 23rd March 2022

DOI: 10.1039/d2ra01346k

rsc.li/rsc-advances

1. Introduction

For many years there have been strong efforts to create so-called hyperpolarized spin systems with polarization far larger than the Boltzmann polarization. Dynamic nuclear polarization[1–4] schemes solve this problem by employing stable radicals or optically created transient triplet states or noble-gases (see *e.g.*, ref. 5–11). Parahydrogen based hyperpolarization schemes employ a chemical reaction of a substrate with parahydrogen[12] for the creation of the hyperpolarization, the so-called parahydrogen induced polarization (PHIP) experiments, which were initially predicted by Bowers and Weitekamp.[13] The first experimental realizations of the experiment were presented in the seminal papers of Weitekamp *et al.*[14,15] and, independently, Eisenberg *et al.*[16] About two decades after the initial discovery of PHIP, Duckett and coworkers[17] proposed a reversible variant of

[a]*Eduard-Zintl-Institut für Anorganische und Physikalische Chemie, Technische Universität Darmstadt, Alarich-Weiss-Str. 8, D-64287 Darmstadt, Germany*
[b]*International Tomography Center, Siberian Branch of the Russian Academy of Science, Novosibirsk 630090, Russia. E-mail: gerd.buntkowsky@chemie.tu-darmstadt.de*

† Dedicated to the memory of our friend and colleague, Prof. Dr Konstantin L'vovich Ivanov, 10 January 1977 to 05 March 2021.

Gerd Buntkowsky received his doctorate in Physics at the FU Berlin in 1991. Afterwards, he changed to chemistry where he habilitated in Physical Chemistry in 2000. In 2004 he became full professor at the FSU Jena. Since 2009, he is Professor of Physical Chemistry (Chair) at the Technical University Darmstadt. His research focuses on the investigation of the structure and dynamics of condensed matter using solid-state NMR techniques and, on the development and application of hyperpolarization techniques in solution and solid-state NMR. He has authored more than 270 publications in these fields.

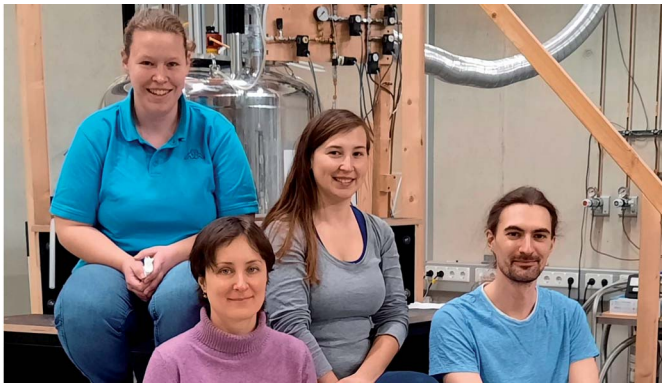

From left to right: Laura Wienands, Yuliya Miloslavina, Franziska Theiss, Jonas Lins.

Franziska Theiss *received her Master of Science degree in chemistry in 2020. In her doctoral studies under the supervision of Gerd Buntkowsky she studies the hyperpolarization of complex molecules with PHIP and polarization transfer at zero and ultra-low fields.*

Jonas Lins *received his master's degree in chemistry in 2019. He then started his PhD studies under the supervision of Dr Gerd Buntkowsky. His work is focused on the synthesis and modification of peptides and the application of the PHIP technique in solution NMR.*

Yuliya Miloslavina *received her PhD at the MPI for Chemical Energy Conversion in 2008. After participating in several European collaborative networks, she started in 2012 to work in the field of NMR in structural biology. In 2021 she joined the Buntkowsky group as senior research fellow, where she works on the development and synthesis of PHIP labelled peptides for non-invasive cancer diagnostics by MRI.*

Laura Wienands *received her master's degree in Bio- and Pharmaceutical Analysis at the Hochschule Fresenius in 2017. In 2018 she started her doctoral studies under the supervision of Gerd Buntkowsky. Her research focuses on the optimisation of protocols and reactions conditions for biophysical or medical applications of PHIP.*

the PHIP reaction, called SABRE (Signal Amplification By Reversible Exchange). In the PHIP techniques, the strong spin order of parahydrogen (p-H_2, the H_2 molecule in its nuclear singlet spin state) is used to generate NMR signal enhancements. It is relatively easy and cheap to produce p-H_2 (enrichment of H_2 with >90% of p-H_2 has become feasible and even standard), and the starting "spin order" of the protons is very high: nearly all H_2 molecules are in the same spin state. In order to render the spin order of the parahydrogen visible in an NMR spectrum, a symmetry-breaking step is needed, which is provided by a chemical reaction. In such a step either p-H_2 is chemically attached to a molecule with an unsaturated C–C bond or the spin order of p-H_2 is transferred to a substrate in a transient organometallic complex. The former scheme corresponds to the conventional PHIP with catalytic hydrogenation, whereas the second scheme is the SABRE experiment.[7] Both variants of PHIP are widely used to enhance NMR signals in general to investigate chemical processes or to enhance the sensitivity in analytical applications.[18,19]

While there is some application overlap between DNP and PHIP in the fields of solution NMR and medical applications, the two techniques are highly complementary. The main advantages of the DNP schemes are that they are versatile, independent of a catalyst, cause no chemical modification of the substrate, and are applicable both in solution and solid-state NMR spectroscopy as well as MRI (see Handbook of high-field DNP[20] and references therein). Their disadvantages, however, are that they depend on a sophisticated and expensive apparatus, need a doping with stable radicals or chromophores and often have to be performed at cryogenic temperatures to achieve efficient levels of hyperpolarization.

The main advantages of PHIP schemes compared to DNP are their independency of any sophisticated experimental hardware and the opportunity to be implemented on any modern NMR spectrometer for few thousands of Euros. An overview of current PHIP instrumentations is given in a recent review by Schmidt *et al.*[21] Other advantages are the use of inexpensive chemical

Alexey Kiryutin studied Chemistry at the Novosibirsk State University and received his doctorate in 2009 under the supervision of Alexandra Yurkovskaya at the ITC. As AvH research fellow, he did a postdoc with Hans-Martin Vieth at FU-Berlin. There he started to explore PHIP at variable magnetic field utilizing field cycling NMR. After returning to the ITC, he develops state of the art field cycling adds-on compatible with NMR spectrometer for relaxation and hyperpolarization study over magnetic field of nine orders. Yurkovskaya and Kiryutin worked for two decades with Konstantin Ivanov on various problems of spin hyperpolarization, relaxation and polarization transfer.

Alexandra Yurkovskaya studied physics at Novosibirsk State University and graduated in chemical physics in 1980. Then she became a researcher at Institute of Chemical Kinetics and Combustion and got her doctoral degree in 1987. She received her second scientific degree in physics (habilitation) in 1997. She was Research Fellow of the Humboldt Foundation (1997–1999) and received a Marie Curie Fellowship (2006–2008) at the Free University of Berlin (group of H.-M. Vieth). Since 1993, she has been working at the International Tomography Center (ITC) in Novosibirsk, where she currently holds the positions of the Chief Research Scientist.

compounds and the fast formation of the polarization within seconds. PHIP schemes can be employed at ambient temperature and are thus easily amenable for kinetic studies. In the simplest way, PHIP/SABRE experiments are done by blowing the p-H_2 gas through the sample containing the substrate and the catalyst to initiate chemical reactions. The main weaknesses of parahydrogen-based hyperpolarization are its dependences on the presence of a hydrogenation catalyst and, in the case of irreversible hydrogenation, the need of a suitable unsaturated precursor which is chemically modified by the reaction.

PHIP experiments were successfully employed for the detailed investigation of mechanistic problems in organic and inorganic synthesis.[22–29] They have an immense application potential in the field of *in situ* gas phase NMR. This technique provides a direct monitoring of heterogeneous catalytic reactions such as *e.g.*, molecular dynamics, hydrogenation of unsaturated bonds in olefins, H/D-isotope exchange reactions, Fischer–Tropsch and Haber–Bosch type reactions.[30–35] They are sensitive monitors for chemical processes in microreactors.[36–38] They can be employed for sensitivity enhancement in time-domain NMR analyzers.[39,40] Owing to the strong dependence of the PHIP enhancement and signal pattern on the value of the polarization field, PHIP measurements are powerful monitors for local fields in field-cycling experiments.[41–45] There are several excellent reviews which explain in detail the experimental techniques and their theoretical background.[46–50] Currently, there is only a limited number of suitable substrates or catalysts amenable for SABRE, most of them contain nitrogen heterocycles like pyridyl, pyridazyl, pyrimidyl or similar groups.[51] These groups are of very high pharmacological interest, due to their ubiquitous presence in biochemically relevant molecules. Typical application examples of SABRE are the hyperpolarization of organic polymers,[52] amino acids and peptides,[45] and keto–enol tautomers.[53] Hövener *et al.*[54] recently reported the so-called PHIP-X (Parahydrogen-Induced Polarization Relayed *via* Proton Exchange) experiment. In this experiment the hyperpolarization is transferred from the hydrogenated substrate to a target molecule *via* chemical proton exchange.

An important issue for all medical *in vivo* applications of PHIP on humans is the efficient separation of the necessary catalysts from the hyperpolarized substrates. While this separation can be easily achieved for gaseous substrates, such as hyperpolarized propene,[55,56] for fluid substrates there is until now no really satisfying answer. Currently there are three possible solutions to this problem, namely (i) the immobilization of an homogeneous catalyst *via* tethering to *e.g.* a silica surface,[57–62] (ii) employing supported MNPs and (iii) physical separation *via* solubility properties,[63] which is discussed in more detail in the application chapter. However, with all these methods great care has to be taken that no metal centers or other potentially harmful fragments leach into the solution.[64,65]

While the main application potential of PHIP is clearly in Chemistry and the Biosciences, there are also a number of "more exotic" applications of PHIP in Physics. To name two recent prominent examples: Based on the concepts of MASER and LASER, Appelt *et al.*[66,67] developed the concept of a p-H_2 pumped RASER (Radiowave Amplification by Stimulated Emission of Radiation), which delivers sub-millihertz resolution in nuclear magnetic resonance. Budker and coworkers have proposed parahydrogen based ultralow-field NMR techniques as part of the cosmic axion spin precession experiment (CASPEr),[68] an NMR-based dark-matter search to probe the axion-fermion "wind" coupling.[69]

Both PHIP and SABRE have a high application potential in the field of hyperpolarized MRI,[63,70–78] where hyperpolarized substances, such as hydroxyethyl propionate, fumarate or succinate, were employed as contrast agents (see *e.g.* the reviews by Hövener *et al.*,[79] Reineri *et al.*[80] and Aime *et al.*[81]).

2. Principles of parahydrogen induced polarization

Parahydrogen and orthohydrogen

Molecular hydrogen is composed of the two spin isomers: parahydrogen (p-H_2) and orthohydrogen (o-H_2). p-H_2 is characterized by the product of a symmetric rotational and the antisymmetric nuclear singlet spin wave function. In contrast to this, orthohydrogen is characterized by an antisymmetric rotational and one of the three symmetric nuclear triplet spin wave functions. In thermal equilibrium at room temperature all four states have practically equal probability, *i.e.*, a relative population of 25% parahydrogen and 75% orthohydrogen. At liquid nitrogen temperature (77 K) the equilibrium is shifted to roughly 50% parahydrogen and 50% orthohydrogen. In thermal equilibrium below 20 K only the ground state of the energetically lower parahydrogen is populated (see Fig. 1). In other words, in thermal equilibrium all molecules are in the nuclear singlet state and the hydrogen gas is fully hyperpolarized.

The spin-conversion from orthohydrogen to parahydrogen is a kinetically hindered process, which is very slow in the absence of suitable catalysts enhancing the spin-conversion. This can be *e.g.*, relaxation by a paramagnetic species[12] or *via* magnetic dipolar interactions due to adsorption to nuclear spins.[82] In the absence of such a catalyst, pure parahydrogen gas is stable in liquid solutions, can be stored for several weeks[83] and used subsequently for hydrogenation reactions.

A sketch of the basic PHIP theory

There are a number of variations of the PHIP technique. They are all based on the original irreversible variants, which were pioneered by the groups of Weitekamp,[13,14] and Eisenberg.[16] In these classic PHIP experiments parahydrogen is added to an unsaturated bond of a molecule mediated by the catalyst. There are two major variants of the experiment, which differ in their reaction conditions. If the hydrogen addition is performed inside the NMR magnet, the acronym PASADENA[84] is used. If the experiment is performed outside the magnet (ideally at 0 T field, in practice close to the earth field), the acronym ALTADENA[15] is employed.

Independent on the actual reaction conditions, the basic irreversible PHIP experiment can be divided into three steps (see Fig. 2A). In the first step, the catalyst, the unsaturated substrate (an alkyne in the example) and the parahydrogen react

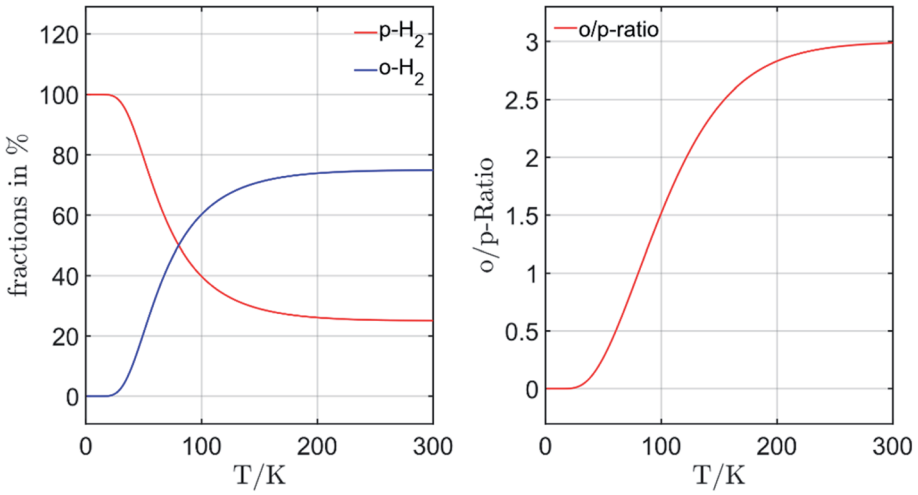

Fig. 1 Equilibrium fractions and ratio of parahydrogen and orthohydrogen as a function of the temperature.

with the rate k_1 to form a transient complex. In the second step, the singlet spin order of the parahydrogen evolves in this transient complex and is – at least partially – converted into visible Zeeman magnetization. In the third step, the transient complex decays to the product (an alkene in the example) and the catalyst with the rate k_2.

There are three similar steps in the case of the reversible PHIP, *i.e.*, SABRE, experiment (see Fig. 2B). In this case, the substrate such as *e.g.*, pyridine, forms a transient complex with the catalyst in the first step. In the second step, the singlet spin order of the parahydrogen is transformed in this complex to the common spin orders of the substrate and the two "nascent" hydride proton spins. In the third step, the complex decays back to catalyst, substrate, and hydrogen.

Polarization and hyperpolarization

The observed intensity of a spectroscopic transition between two energy levels is proportional to their population difference. In the case of the two levels (α and β) of an NMR spin-1/2 system, a relative measure of this population difference is

$$P = \frac{p_\alpha - p_\beta}{p_\alpha + p_\beta}. \quad (1)$$

In thermal equilibrium in the presence of the Zeeman-interaction with a field of B_0 the equilibrium polarization is

$$P_{eq} = \tanh\left(\frac{\hbar\gamma B_0}{2k_B T}\right) \ll 1. \quad (2)$$

Even for protons at the highest currently available fields of 28.2 Tesla, corresponding to 1.2 GHz of proton Larmor

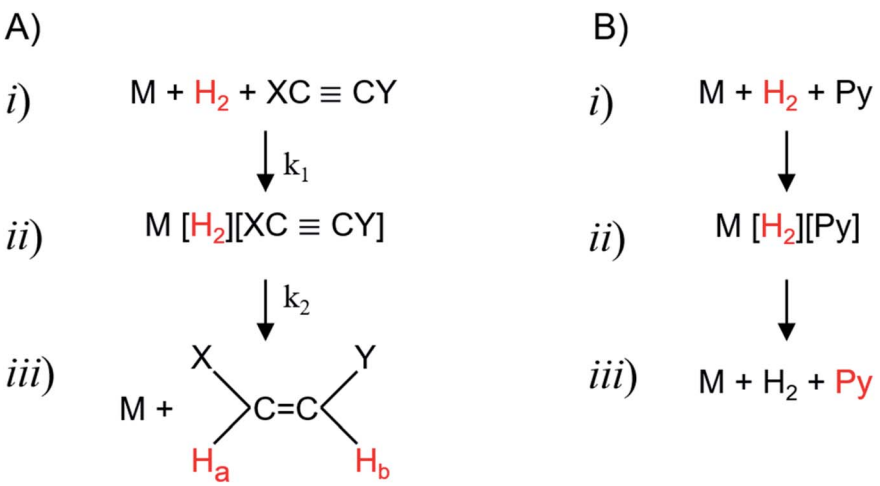

Fig. 2 Basic reaction pathways of the catalyzed hydrogenation in a PHIP (A, irreversible) and SABRE (B, reversible) reaction. (i) The unsaturated precursor, respectively the SABRE substrate, such as pyridine Py as example, reacts with parahydrogen (marked red) and the catalyst M to form the intermediate (ii), which can be, *e.g.*, a dihydride or dihydrogen complex. In the case of PHIP, this complex decays into the hyperpolarized product (iii) and the catalyst (see ref. 85 for details). In the case of SABRE, the hyperpolarization of the parahydrogen is (at least partially) transferred to the substrate.

frequency, the equilibrium polarization at 300 K is only about $P_{eq}(^1H) \approx 9.6 \times 10^{-5}$. The situation is even worse for X-nuclei such as *e.g.*, ^{13}C, where the lower gyromagnetic value reduces this to $P_{eq}(^{13}C) \approx 2. \times 10^{-5}$. In order to achieve higher polarization while being able to measure at ambient temperature, it is necessary to bring the spin system in a hyperpolarized state, which is very far away from thermal equilibrium. The typical measures for this hyperpolarized state are the polarization value P_{hyp} itself, or the enhancement factor

$$\varepsilon = \frac{P_{hyp}}{P_{eq}}. \quad (3)$$

Basic ^{1}H–PHIP theory of a two-spin system

A detailed discussion of the various variants of the PHIP experiment is beyond the scope of the present review. In the following only the basic theory for a two-proton system is sketched. More details are found *e.g.*, in the reviews by Bowers and Weitekamp[86] or Canet *et al.*[87]

The initial state of a PHIP experiment is created by a chemical reaction of the parahydrogen with the substrate molecule R

$$R + pH_2 \rightarrow P \quad (4)$$

to form the product P. From the point of view of the spins, the chemical reaction is a sudden change of the spin Hamiltonian from parahydrogen Hamiltonian ($J_{para} \approx 3.65 \times 10^{12}$ Hz)

$$\hat{H}_{para} = J_{para}(\hat{S}_x\hat{I}_x + \hat{S}_y\hat{I}_y + \hat{S}_z\hat{I}_z) \quad (5)$$

to the spin Hamiltonian of the reaction product (ν_S,ν_I: nuclear Zeeman frequencies; $J \approx$ 1–20 Hz scalar coupling constant)

$$\hat{H} = \nu_S\hat{S}_z + \nu_I\hat{I}_z + J(\hat{S}_x\hat{I}_x + \hat{S}_y\hat{I}_y + \hat{S}_z\hat{I}_z). \quad (6)$$

Starting point for the NMR description is the spin density matrix of the parahydrogen, which corresponds to the singlet state. It can be written as

$$\hat{\rho}_p = \frac{1}{4}\hat{E} - \left(\hat{S}_x\hat{I}_x + \hat{S}_y\hat{I}_y + \hat{S}_z\hat{I}_z\right). \quad (7)$$

Here $\{\hat{I}_k,\hat{S}_k\}$, $k = x, y, z$, are the spin operators of the two protons from the parahydrogen molecule, and $\hat{E}$ is a unity operator. As long as the two spins are magnetically equivalent, *i.e.*, have the same Larmor frequency ($\nu_S = \nu_I = \nu_0$), this density operator commutes with the spin Hamiltonian

$$\hat{H}_0 = \nu_0(\hat{S}_z + \hat{I}_z) + J(\hat{S}_x\hat{I}_x + \hat{S}_y\hat{I}_y + \hat{S}_z\hat{I}_z), \quad (8)$$

i.e.,

$$[\hat{H}_0,\hat{\rho}_p] = 0 \quad (9)$$

and $\hat{\rho}_p$ does not change. In the singlet state the two protons don't give an NMR signal, since

$$[\hat{S}_k + \hat{I}_k, \hat{\rho}_p] = 0, k = x, y, z. \quad (10)$$

The situation changes, when the two spins become inequivalent, *i.e.*, when they have different Larmor frequencies. In the case of a two-spin system, this inequivalence stems from chemical shift differences. For larger systems they can also be the result of scalar couplings to other spins. In this case the spin Hamiltonian is

$$\hat{H} = \nu_S\hat{S}_z + \nu_I\hat{I}z + J(\hat{S}_x\hat{I}_x + \hat{S}_y\hat{I}_y + \hat{S}_z\hat{I}_z). \quad (11)$$

Its commutator with the singlet spin density matrix of the parahydrogen is no longer zero,

$$[\hat{H},\hat{\rho}_p] = i(\nu_S - \nu_I)(\hat{S}_x\hat{I}_y - \hat{S}_y\hat{I}_x). \quad (12)$$

Thus, the density matrix becomes time dependent as soon as the symmetry of the spins is broken by the reaction. Before the actual NMR experiment, the reactions run for typically a few to a few tens of seconds. Because of this finite reaction time all the oscillations are damped out and the initial condition of the experiment at the end of the reaction time is ($\Delta\nu := \nu_S - \nu_I$):[49]

$$\hat{\rho}_{eq} = \frac{1}{2}\begin{pmatrix} 0 & 0 & 0 & 0 \\ 0 & 1 - \frac{\Delta\nu\, J}{J^2 + \Delta\nu^2} & -\frac{J^2}{J^2 + \Delta\nu^2} & 0 \\ 0 & -\frac{J^2}{J^2 + \Delta\nu^2} & 1 + \frac{\Delta\nu\, J}{J^2 + \Delta\nu^2} & 0 \\ 0 & 0 & 0 & 0 \end{pmatrix}. \quad (13)$$

In particular, for an AX spin system with $\Delta\nu \gg J$ one obtains simply as initial condition

$$\hat{\rho}_{eq,AX} = \frac{1}{2}\begin{pmatrix} 0 & 0 & 0 & 0 \\ 0 & 1 & 0 & 0 \\ 0 & 0 & 1 & 0 \\ 0 & 0 & 0 & 0 \end{pmatrix}. \quad (14)$$

In other words, only the spin-states αβ and βα are populated, and the population differences to the levels αα respectively ββ, which are relevant for the intensities of the NMR signals, are on the order of unity instead of on the order of 10^{-5}, *i.e.*, four to five orders of magnitudes larger.

Singlet–triplet conversion of hydrogen in PHIP

Konstantin Ivanov proposed, in analogy to the well-known spin-correlated radical pair model from Spin Chemistry[88] explaining the origin of the chemically induced dynamic nuclear polarization (CIDNP),[89–92] a pictorial description of the spin-dynamics of the spin-pair (see in Fig. 3). As outlined above, at high magnetic field this proton spin pair undergoes a time dependent spin interconversion with the central triplet T_0 state. Singlet and central triplet states are not eigen states of two spin-1/2 system at high magnetic fields, therefore fast oscillations take place between them. These states are invisible by a conventional NMR; however, recently it was proven that singlet–triplet conversion indeed takes place in parahydrogen reversibly bound to a complex[88] and gives rise to formation of orthohydrogen. This process is remarkably efficient and

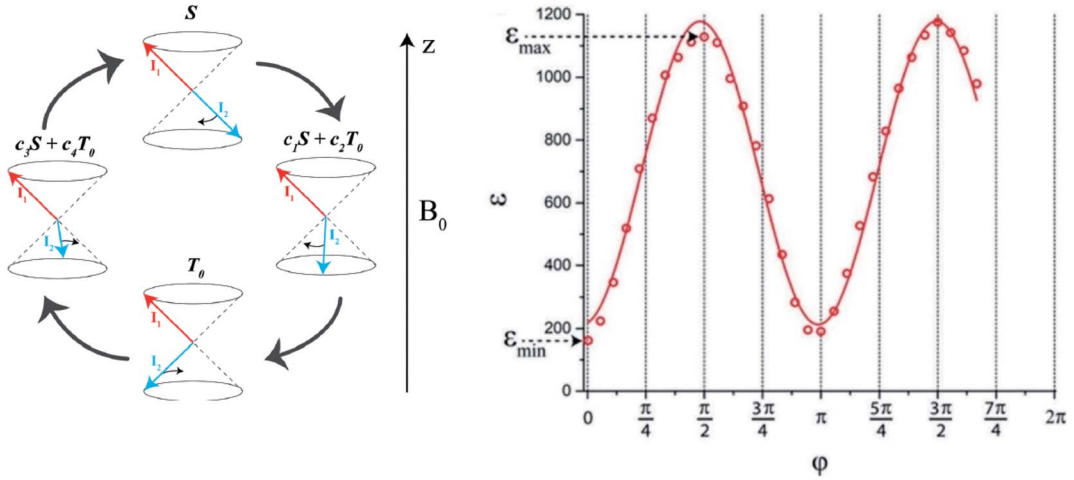

Fig. 3 Left: Diagram explaining singlet–triplet conversion for $\Delta\nu \neq 0$. The red and blue arrows stand for the spin vectors of the two protons, the S state is the state with anti-parallel spins. While the total spin in the T_0 state is nonzero, its z-projection is zero. The spins precess about the B_0 field at different frequencies: faster precession of one of the spins (for simplicity, we assume that only I_2 precesses) gives rise to coherent S–T_0 mixing, *i.e.*, S goes to a superposition of S and T_0, then to T_0, then again to a superposition and so on. Right: The dependence of ^{15}N signal enhancement of the deuterated ^{15}N-enriched pyridine on the flip angle φ of non-selective proton pulse. For details see ref. 88.

strongly reduces the achievable NMR signal enhancement of a substrate (in the analyzed case the ^{1}N nuclei of pyridine). Clear evidence that singlet–triplet conversion in the bound H_2 plays an important role in SABRE experiments was taken from the nutation angle dependence of the ^{15}N signal enhancement shown in Fig. 3. Due to the magnetic non-equivalency of two "nascent" hydride spins in their chemical shifts and spin–spin interactions with nuclear spins of substrate in the complex, this singlet–triplet conversion is sensitive to the spin orientation of the substrate spin as well. As result, the singlet–triplet conversion becomes faster in the catalytic iridium complex with ^{15}N enriched substrates. At high field, the other important consequence of this interconversion is that it favors only one of the three triplet states, here the central triplet state T_0, producing polarized o-H_2 that does not obey a Boltzmann distribution. The latter gives rise to the possibility of the ultrasensitive indirect NMR detection of catalytic hydrogen complexes, as suggested in ref. 93 (see Chapter 3).

^{1}H–PHIP of larger spin systems

The situation is more complicated in larger spin systems, where analytical solutions are generally not available. However, as long as longitudinal relaxation processes can be neglected, it is relatively easy to estimate the initial conditions numerically by a truncation[94] approach, where the transformed density matrix is averaged over the reaction time T

$$\hat{\rho}_{\mathrm{eq,gen}} = \frac{1}{T}\int_0^T \exp\left(-i\hat{H}t\right)\hat{\rho}_{\mathrm{p}}\exp\left(-i\hat{H}t\right)\mathrm{d}t, \qquad (15)$$

which removes all oscillating terms from the density matrix. In this case, the population of the initial singlet state will be distributed in general over more levels, but the population differences will still be orders of magnitude larger than the thermal equilibrium polarization.

Proton detected PHIP

The most common way to detect PHIP hyperpolarization is by ^{1}H-NMR. The actual line-shape of the spectra depends on the spin system, the employed pulse sequence, the strength of the external magnetic field during the hydrogenation and during the detection, the switching time between the fields and kinetic processes in the reaction intermediate. There are several excellent reviews on the ^{1}H-detected variant of PHIP.[26,46,86,95]

The conversion of singlet spin order into nuclear spin order during the hydrogenation reaction leads to typical polarization patterns in the NMR spectra of the hydrogenation products, which depend on the spin system and its parameters, such as chemical shifts, scalar couplings, the strength of the external magnetic field during the reaction and the type of field change (*e.g.*, adiabatic, or sudden change). Ivanov *et al.*[96] obtained analytical solutions for several types of coupled three spin systems and calculated the effect of the external magnetic field strength on the PHIP signal for them. This dependence is demonstrated in the simulations of Korchak *et al.*[42] They have calculated the effect of the external magnetic field strength on the PHIP signal for a three spin system (see Fig. 4). It is evident that the signal pattern changes drastically with the strength of the polarization field or the type of field change (adiabatic *versus* sudden change). Kiryutin *et al.*[97] analyzed the effects of nuclear spin level anti-crossings on the PHIP pattern. They found that rapid passage through the level anti-crossing enables highly efficient polarization transfer between specific spin orders, and that in general, the experimental protocol for the variation of the magnetic field is a means for manipulating PHIP patterns and transferring polarization to target spins of choice.

PHIP detected by X-nuclei

Owing to the comparable short relaxation time of proton polarization, which is typically on the time scale of few seconds,

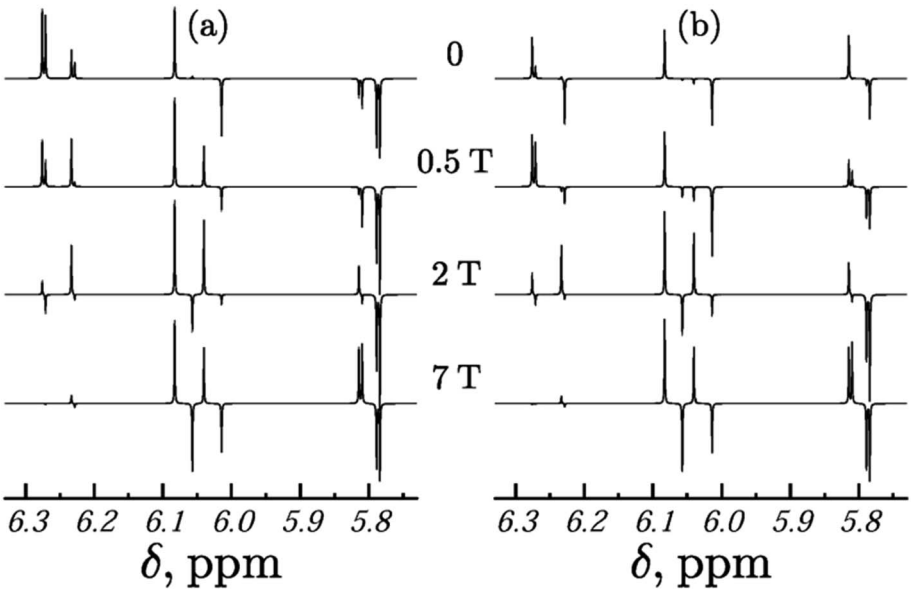

Fig. 4 PHIP spectra of a three-spin system calculation for different reaction fields at a detection field of 9.4 T. (a) Adiabatic (slow), (b) sudden field variation. Parameters of the calculations: $\varphi = \pi/4$; δ = {5.8 ppm, 6.05 ppm, 6.25 ppm}; $J_{1,2} = 10.5$ Hz; $J_{1,3} = 1.8$ Hz; $J_{23} = 17.2$ Hz. Figure reproduced from Korchak *et al.*[42] (reproduced from ref. 42 with permission from the Royal Society of Chemistry, copyright 2009).

it is advantageous to transfer the hyperpolarization to an X-nucleus, such as ^{13}C, where the life-time of the hyperpolarization is typically an order of magnitude longer, which strongly enhances the application window of the hyperpolarization. Initial applications employed INEPT type experiments to exploit this idea and developed the PH-INEPT sequence as a very efficient tool to hyperpolarize the X-nuclei.[4,98,99] An overview about these techniques is given by Kuhn and Bargon.[100] Bernarding *et al.*[75,101,102] described the hyperpolarization of ^{19}F containing substrates, which has a high application potential as contrast agent in MRI, as there is practically no ^{19}F background in living tissue. Glöggler *et al.*[103,104] reported a pulsed transfer experiment, which can nearly completely transfer the hyperpolarization from the protons to the ^{13}C. Theis *et al.*[105] discussed SABRE hyperpolarization for sensitivity enhancement of rare X-nuclei. Ivanov *et al.*[106] proposed the INEPT-SABRE sequence for polarization transfer in SABRE experiments and developed a number of versatile tools based on utilizing level-anti-crossing (LAC) in the rotating frame for transferring spin hyperpolarization. The LAC conditions can be fulfilled by applying resonant RF-excitation at the NMR frequency of the protons and the heteronuclei without necessity to utilize magnetic field cycling. Highly efficient conversion of para-hydrogen-induced polarization into net polarization of spin-1/2 insensitive nuclei by adiabatic passage through the level anti-crossings (LACs) in the doubly rotating frame of reference was demonstrated for ^{13}C in ref. 107 and for ^{15}N in ref. 108 The dependence of the polarization transfer efficiency on the RF-field parameters and on the time profile of switching off the RF-field has been studied in detail; experimental results are in excellent agreement with the theory developed.[109]

The Side Arm Hydrogenation (PHIP-SAH) by Reineri *et al.*[110] opened up a new range of hyperpolarized molecular probes. In this approach the molecule of interest is functionalized with an unsaturated moiety (the "side arm"[111]) which is chemically removed after hydrogenation with p-H_2 and further transfer of the hyperpolarization to the ^{13}C target signal. Its power was demonstrated recently by the Reineri group employing hyperpolarized [1-^{13}C]pyruvate,[112] to detect *in vivo* maps of pyruvate and its metabolic product lactate on a 1 T MRI scanner. An overview on this technique is found in a number of recent reviews.[79]

Reversible PHIP (SABRE)

In the reversible PHIP (SABRE) scheme,[17] a transient complex of parahydrogen, the substrate and a suitable organometallic complex, which induces the polarization transfer from the parahydrogen to the substrate, is formed. The latter is usually an N-heterocyclic carbene (NHC) complex.[113] In this complex the hyperpolarization is transferred from the parahydrogen to the substrate through scalar couplings in the complex.[114] Later the complex dissociates again into substrate, dihydrogen and catalyst, causing a hyperpolarization of the substrate reservoir. A major advantage of the SABRE scheme is that no substrate is consumed, and many hyperpolarization cycles can be performed, thus allowing a substantial amount of the substrate to be hyperpolarized by "pumping" polarization into the substrate reservoir. The final level of hyperpolarization depends on the production and the relaxation rates of the SABRE process. This hyperpolarization is then used for the NMR detection. Afterwards, as no substrate is consumed, the same molecules can be hyperpolarized again by bubbling new parahydrogen through the solution.

A simple phenomenological model of the polarization transfer processes was given by Barskiy *et al.*[115] Quantitative

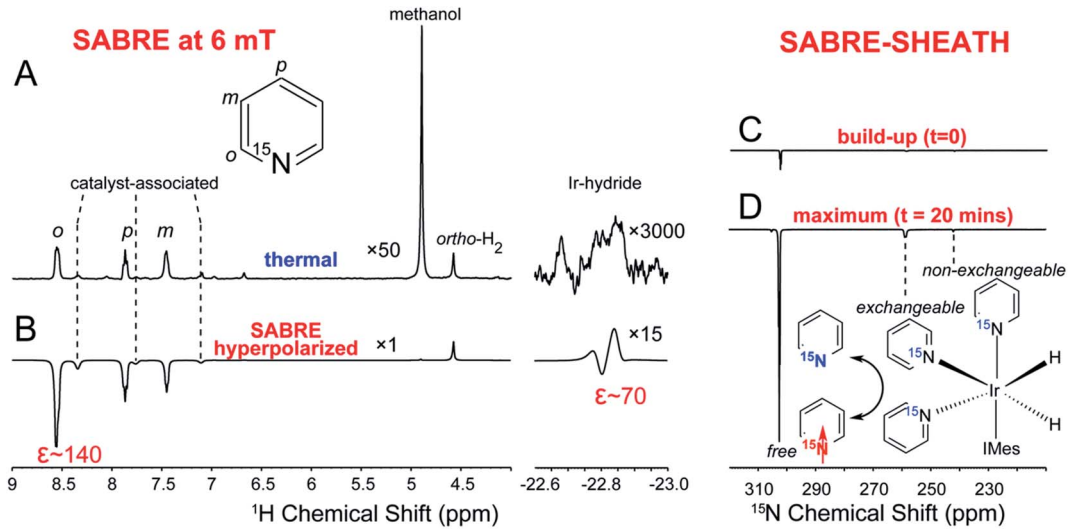

Fig. 5 ^{1}H and ^{15}N NMR spectroscopy of SABRE catalyst activation and ^{15}N SABRE-SHEATH build-up. (A) ^{1}H thermal NMR spectrum of 2 mM activated Ir-IMes catalyst solution with 48 mM ^{15}N-pyridine. (B) ^{1}H spectrum of hyperpolarized ^{15}N-pyridine *via* conventional low-field (6 ± 4 mT) SABRE. The resonances labeled with dashed lines correspond to catalyst-associated pyridine.[59] (C and D) ^{15}N NMR spectra of ^{15}N-pyridine hyperpolarized by SABRE-SHEATH at micro-Tesla fields. (C) NMR spectrum of ^{15}N-pyridine ($\varepsilon_{free} \sim 300$) sample corresponding to completely activated catalyst solution (as validated by ^{1}H NMR using conventional lowfield SABRE through achieving efficient enhancement of pyridine proton polarization, and also validated through *in situ* detection of the disappearance of SABRE hyperpolarized Ir-hydride intermediate species). (D) ^{15}N NMR spectrum of ^{15}N-pyridine sample corresponding to maximum SABRE-SHEATH signal intensity ($\varepsilon_{free} \approx 3600$) achieved with ~20 min of para-H_2 bubbling. This figure has been adapted from ref. 120 with permission from the American Chemical Society (ACS), copyright 2015.

theoretical description of the SABRE process with rigorous consideration of spin dynamics, level anti-crossings (LACs) and chemical exchange was proposed by Knecht *et al.*[116,11] A detailed discussion of these models is given in the review by Ivanov *et al.*,[118] which includes an extensive list of SABRE active substrates. In the following the salient elements of this description are summarized.

The crucial step in the SABRE process is the polarization transfer from the bound parahydrogen nuclei to the nuclei of the substrate. This transfer can occur either as a direct process *via* the scalar coupling connecting the two nuclei or as a relayed process, where the polarization is transferred in steps: first to nearby and stronger coupled nuclei and then to the nuclei of interest. A theoretical approach to SABRE-relay, which can treat both spin dynamics and chemical kinetics as well as the interplay between them, and allows optimization of SABRE-relay experiments with the ultimate goal of achieving maximal NMR signal enhancements for substrates of interest, was developed by Ivanov *et al.*[119]

Polarization transfers between protons at high magnetic field are energy conserving with respect to the dominating Zeeman interaction and occur fast under the influence of the scalar interactions. In contrast, transfers from protons to heteronuclei such as *e.g.*, ^{15}N, are inefficient, as the Zeeman energy is not conserved.

If the hyperpolarization is to be transferred to an X-nucleus, it is necessary to remove this Zeeman barrier and bring the two spin-reservoirs into contact. The easiest solution for establishing the contact is to perform the SABRE experiment at very low magnetic fields, where the Zeeman energies are small and efficient polarization transfer is feasible. The resulting experiment is called SABRE-SHEATH (SABRE in Shield Enables Alignment Transfer to Heteronuclei). It achieves the polarization transfer in the case of N-heterocyclic substrates, such as pyridine-^{15}N, at fields of typically 0.2–0.6 μT.[120] At these fields there are LACs, which cause a strong mixing of the spin-states of the protons and the ^{15}N-nuclei, and enable the transfer, as explained by Ivanov *et al.*[121]

At high magnetic fields alternative transfer mechanisms to X-nuclei are needed. This can be achieved *e.g.*, by the creation of anti-phase polarization (see review by Ivanov *et al.*[118] and references therein) or *via* RF irradiation on the complex. The latter schemes are summarized under the acronym RF-SABRE. Typical examples of it are the LIGHT-SABRE (Low-Irradiation Generation of High Tesla-SABRE)[122] and the SLIC-SABRE (Spin Lock Induced Crossing SABRE)[123–125] experiments.

The essential optimization of the RF-SABRE performance for low γ nuclei as proposed by Ivanov *et al.*[106] is based on the utilization of the shaped RF pulses with constant adiabaticity. Based on the concept of LAC, they implemented adiabatic RF-field variation to optimize the sweeping profile in order to (a) minimize the time and (b) keep a high degree of adiabaticity. Qualitatively, this can be achieved by slowly passing through the LAC regions in rotating frame and introducing fast passage in-between LACs (see ref. 106 for details). The recent development of this approach deals with the highly efficient transfer of proton hyperpolarization to low γ nuclei by adiabatically sweeping the external magnetic field.[126,127]

Fig. 5, adapted from Chekmenev *et al.*,[120] displays several of these SABRE effects, employing ^{15}N labeled pyridine as

substrate. The upper panel compares the thermal (A) and the SABRE hyperpolarized (B) signals of the free and the complex bound pyridine protons. The lower panel displays the ^{15}N-signal of the pyridine, obtained by SABRE-SHEATH (C and D).

PHIP and SABRE at zero to ultra-low-field

An alternative approach for the hyperpolarization of X-nuclei is the zero-to-ultra-low-field nuclear magnetic resonance (ZULF-NMR) technique, where weak magnetic fields in the range of few nanotesla (nT) are employed.[128–134] At these ultra-low-fields the Zeeman-Interaction is on the order of few tenths or hundreds of millihertz (mHz), which is much smaller than the size of typical scalar interactions between nuclear spins. This creates a strongly coupled spin system, whose eigenstates are determined by the scalar interaction Hamiltonians and no longer by the Zeeman Hamiltonian. As example we consider a spin system consisting of two spin-species I and S, such as *e.g.*, ^{1}H and ^{13}C. The relevant Hamiltonian of the spin system at ultra-low field $B = B_{UL}$ is the sum of the Zeeman terms and the scalar interactions

$$\widehat{\mathscr{H}} = -\omega_I \sum_i \hat{I}_{iz} - \omega_S \sum_i \hat{S}_{iz} + 2\pi \sum_{i>j} J_{ij}^{II} \left(\hat{\mathbf{I}}_i \cdot \hat{\mathbf{I}}_j\right) + 2\pi \sum_{i>j} J_{ij}^{SS} \left(\hat{\mathbf{S}}_i \cdot \hat{\mathbf{S}}_j\right) + 2\pi \sum_{i,j} J_{ij}^{IS} \left(\hat{\mathbf{I}}_i \cdot \hat{\mathbf{S}}_j\right). \quad (16)$$

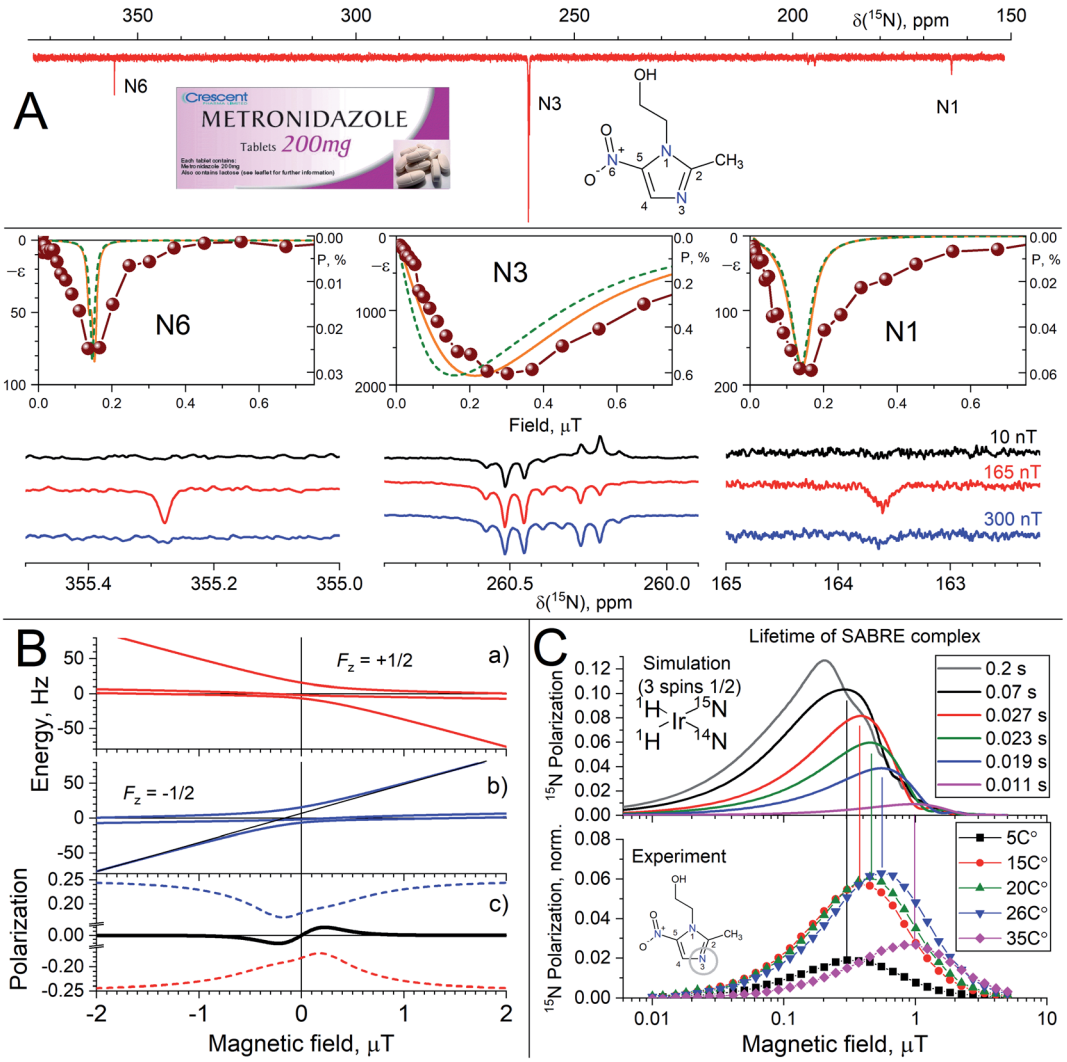

Fig. 6 (A) ^{15}N SABRE in DMSO-d_6, showing the difference in field dependence of nitrogen atoms in one molecule (central part) and representative NMR spectra (lower part). ^{15}N NMR spectrum of polarized metronidazole at 0.165 μT with proton decoupling is shown in the upper part. Lines show the calculation result, which takes into account four (solid orange) and three (green dash) interacting spins in active complex. (B) Energy levels of a three-spin system – two protons HH′ coupled to a ^{15}N nucleus – at ultralow fields. ^{15}N polarization generated by spin mixing in the $F_z = +\frac{1}{2}$ and $F_z = -\frac{1}{2}$ state manifolds (red and blue dashed lines, respectively) and the total ^{15}N polarization (solid black line). (C) ^{15}N SABRE field dependence for N3 at ultralow fields at variable temperature: simulation (upper plot) and experimental data (lower plot). For details see Kiryutin *et al.*[135]

Here $\omega_k = -\gamma_k \times B_{UL}$, k = I, S is the angular frequency of the Zeeman interaction of the spins and J_{ij}^{II}, J_{ij}^{SS}, J_{ij}^{IS} are the homonuclear and heteronuclear scalar-coupling constants. The sum-indices *i*,*j* run over all proton respectively carbon spins in the spin system. At ultra-low fields, the difference in Larmor frequency $\{\omega_I - \omega_S\}/2\pi$ between I and S spins is much smaller than the heteronuclear coupling constants, J_{ik}^{IS}. Thus, there is no longer a difference between homo- and heteronuclear spin and the usual distinction between protons and X-nuclei is lifted. As a consequence, polarization can be transported between the I and S nuclei by means of the IS-scalar interactions and later detected at high-field *via* field-cycling.

Kiryutin *et al.*[135] recently presented an advanced study of SABRE generated ^{15}N polarization of metronidazole *via* spin mixing at ultralow magnetic fields at natural ^{15}N isotope abundance. The most efficient polarization transfer from protons to low γ of nuclei S occurs at the level-crossing condition $\{\omega_I - \omega_S\}/2\pi = J_{ik}^{IS}$. The temperature variation revealed crucial difference between SABRE polarization generated for three N-atom positions in metronidazole: only one of them, namely N3, can be directly bound to the SABRE catalyst, while the other two ^{15}N spins get polarization indirectly *via* coupling to protons of the polarized substrate. As an experimental example of this technique, Fig. 6 displays a magnetic field dependence of metronidazole and natural abundance of ^{15}N. The signal enhancements are reaching 46 000 (15% polarization) for the most efficiently polarized N3-atom. In contrast to the other nitrogen positions, its optimum polarization field strongly depends on the sample temperature, which affects the kinetic parameters (describing SABRE complex formation and dissociation, lifetime of the active polarization transfer complex, τ_d), but not the spin Hamiltonian (Fig. 6).

This observation is explained by the fact that the SABRE field dependence is conditioned by LACs at zero field, which become lifetime broadened. Hence, the LAC-based analysis of SABRE remains valid, although in some cases – like the one studied here – not only the LAC position but also the LAC width becomes important. The width of LAC is conditioned by chemical dynamics of reversible binding that was rigorously described by Knecht *et al.*[116,119] Such a lifetime broadening of the LAC provides interpretation of the data presented in Fig. 6: upon temperature variation the τ_d value is strongly affected. Consequently, ΔB_{LAC} changes and so does B_{max}. This assumption is in agreement with the calculation of the SABRE field dependence performed for variable complex lifetime τ_d: when τ_d becomes short at elevated temperature, the B_{max} value increases (see Fig. 6C). The effect of the lifetime becomes important when the product of τ_d and the characteristic spin mixing frequency ν_{mix} is smaller than 1; otherwise B_{max} is determined by the J_{eff} parameter.

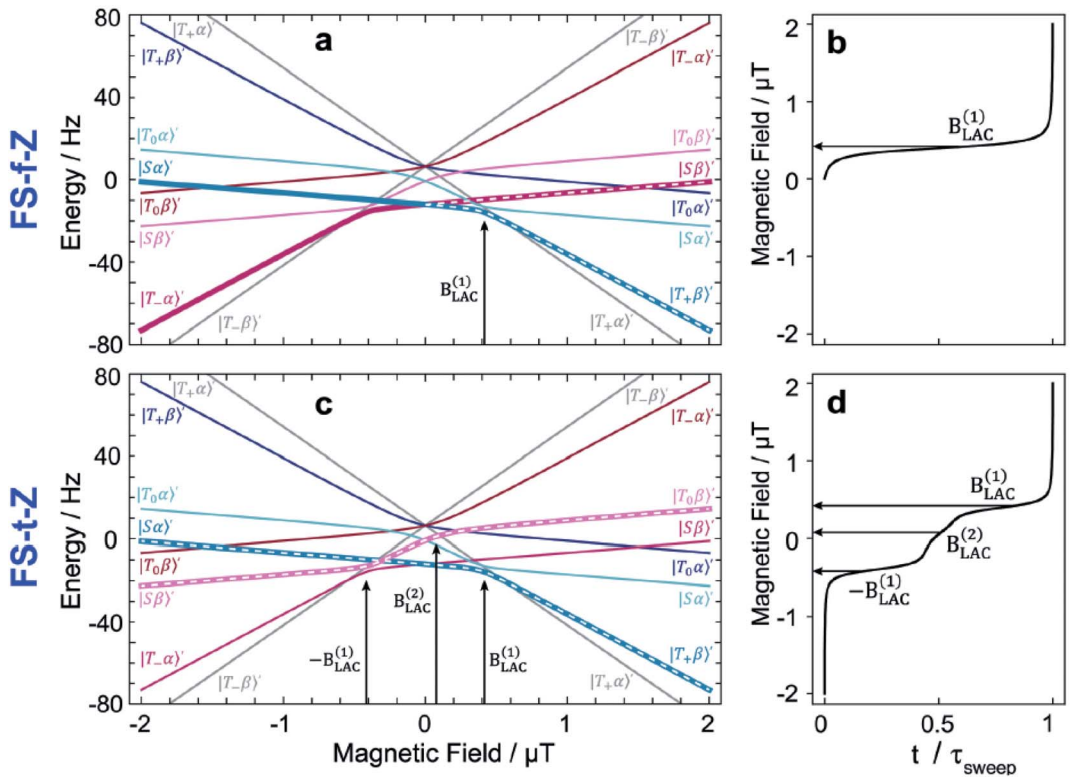

Fig. 7 Eigenvalue plots for the 3-spin system of [1-^{13}C]fumarate with state labels shown. (a) Relevant energy levels for the field sweep from zero field (FS-f-Z) experiment are highlighted with white dashes, and the one relevant LAC is labelled. (b) Constant-adiabaticity profile. (c) Relevant energy levels for the field sweep through zero field (FS-t-Z) experiment are highlighted, and the three relevant LACs are labelled. (d) Constant-adiabaticity profile. Colors distinguish between state manifolds with different angular momentum projection (grey: $m = \pm 3/2$; blue: $m = +1/2$; red: $m = -1/2$). For details see Rodin *et al.*[126] (reproduced from ref. 126 with permission from the Royal Society of Chemistry, copyright 2021).

The key parameter of PHIP experiments at ultralow fields with detection at strong magnetic field is the rate of the magnetic field switching as compared with the coupling parameter among nuclei. In general, it can be slow (adiabatic), sudden (non-adiabatic)[136] or mixed. For the maximal polarization of PHIP and SABRE substrate, it is necessary to switch the magnetic field adiabatically, but as quickly as possible in order to reduce the relaxation effect. Ivanov *et al.*[126,127] proposed the optimized methods for adiabatic field switching for ultralow fields: the so-called field cycling (FC) and field sweeping (FS) methods called FS-f-Z and FS-t-Z, meaning field switching *from* zero and *through* zero (Fig. 7).

Previously, such methods used either uncontrolled switching of the magnetic field, for example, taking the sample out of the magnetic shield, or linear switching of the magnetic field, which is not the optimum form for ensuring fast and efficient polarization transfer. The point is that on the one hand the field switch should be as fast as possible but on the other hand the field has to change slowly in the LAC regions. Ivanov *et al.*[126] proposed a switching profile that meets this requirement and provides faster and more efficient polarization transfer (see Fig. 7). They have demonstrated this by the example of polarization transfer from the proton singlet order to the ^{13}C magnetization in PHIP-polarized [1-^{13}C]fumarate obtained from the precursor by hydrogenation with parahydrogen. To provide this shape, we proposed a profile of field variation with a constant adiabaticity parameter ξ, which was previously used to improve methods for generating long-lived singlet order[137]

$$\xi(t) = \sqrt{\sum_{ij} \xi_{ij}^{\,2}(t)}, \quad \text{where } \xi_{ij}(t) = i\left|\partial_t \hat{H}\right|j\Big/\omega_{ij}^{\,2}. \qquad (17)$$

Here (i,j) denote the eigenfunctions of the complete Hamiltonian $\hat{H}$, ω_{ij} – the energies difference of these levels. The field switching profiles for the FS-f-Z and FS-t-Z methods, obtained using the final formula for the specific molecule fumarate, are shown in Fig. 8.

As can be seen from the experimental results (Fig. 8), a profile with a constant adiabaticity parameter makes it possible to achieve a maximum of polarization transfer in a shorter time, which makes it possible to reduce relaxation losses and increase the overall quality of polarization transfer.

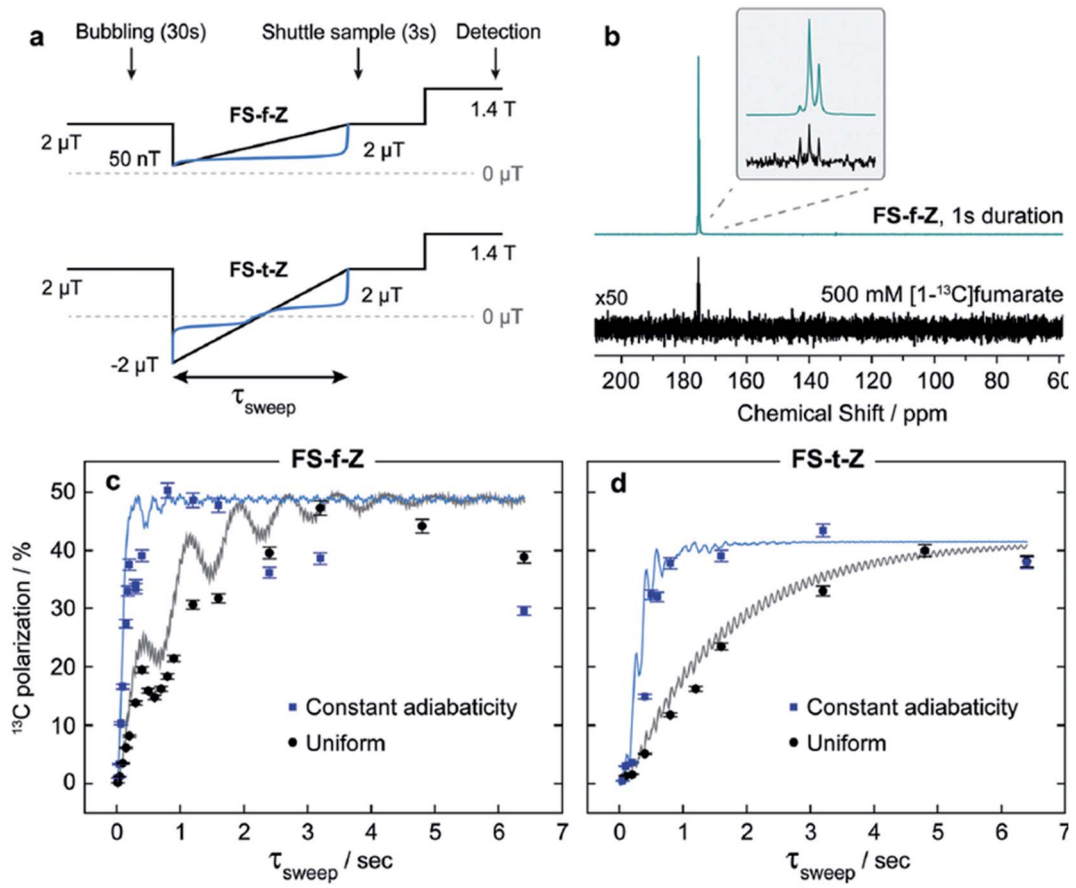

Fig. 8 Optimization of polarization transfer by adiabatic profiles of magnetic field sweep. (a) Experimental protocols for uniform linear (black) and constant-adiabaticity (blue) field sweeps; b) Comparison of hyperpolarized and thermal equilibrium ^{13}C NMR spectrum of 500 mM [1-^{13}C] fumarate in D_2O. The asymmetry in the triplet structure in the hyperpolarized spectrum is due to the nonthermal proton spin polarization. (c and d) Results from the field sweep experiments, contrasting constant-adiabaticity and linear magnetic field profiles for field sweep from zero field (FS-f-Z) and field sweep through zero field (FS-t-Z) experiments. Simulations are shown by the lines fitted to the data. For details see Rodin *et al.*[126] (reproduced from ref. 126 with permission from the Royal Society of Chemistry, copyright 2021).

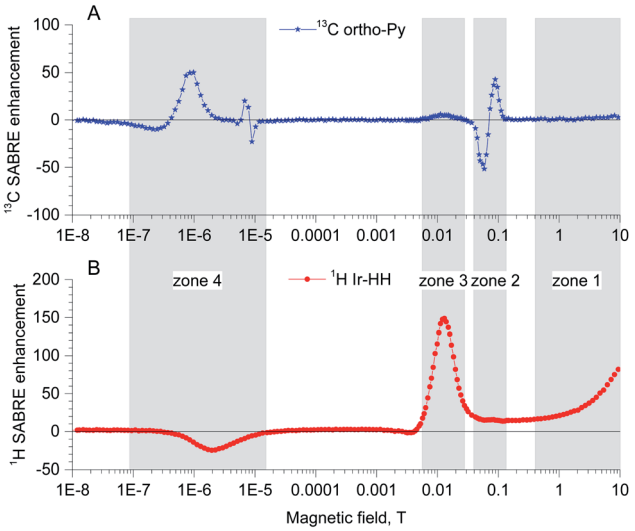

Fig. 9 (A) ^{13}C SABRE field dependence for ortho carbon of ^{15}N-pyridine, for details see ref. 142. (B) ^{1}H SABRE field dependence for hydride protons on Imeslr-catalyst (unpublished results provided by A. Kiryutin).

Also, these methods are not very sensitive to the uniformity of the longitudinal and transverse fields (compared to coherent methods), which also improves their potential attractiveness as a new and general method for transferring a singlet hyperpolarized order to a heteroatom near LAC region at ultralow magnetic fields. These results make it possible to use profiles with constant adiabaticity for all PHIP experiments with field cycling, where after the addition of parahydrogen a strong coupling between protons and heteronuclei remains and the protons are in a state close to the equivalence.

SABRE polarization in a wide field range

In the previous sections we have seen examples for SABRE at very low fields and at high fields. In a series of papers[138–142] the Ivanov group has analyzed the full field dependence of SABRE. They found that there are four different field regimes (see Fig. 9).

Zone 1 is the regime of high field of NMR spectrometers: the SABRE polarization on hydride protons and on free hydrogen at high field increases proportionally to the magnetic field.[138] In this regime the polarization transfer can be split into 3 steps: (i) generation of the $I_{z1}I_{z2}$ spin order of Ir-HH; (ii) spin conversion of $I_{z1}I_{z2}$ to $I_{z1}+I_{z2}$, leading to generation of net polarization of Ir-HH; (iii) transfer of net polarization Ir-HH to the nearest nuclei (*e.g.*, protons of substrate) by dipolar cross-relaxation.

Zone 2 is a narrow field range from *ca.* 30 mT to 0.2 T. In this regime very strong multiplet polarization on ^{13}C nuclei with strong direct spin–spin couplings on the order of hundred Hz is observed. At these fields no net polarization of the carbons is created. Instead, multiplet proton–carbon polarization is formed *via* LACs, which determine the SABRE field dependence. In particular, the position of the sharp feature in the magnetic field dependence scales by direct J_{CH} spin–spin constant.

Zone 3 with magnetic fields from 5 to 30 mT are typical conditions for the direct proton SABRE polarization transfer from hydrides to protons of bound substrate. *E.g.*, the seminal discovery of proton SABRE by Duckett *et al.*[17] was done in the field of 20 mT. Later the position was theoretically explained[139] and experimentally proved by thorough measurements in a wide field range.[142] In a simple three spin model AA′B, where A and A′ are the chemically equivalent protons attached to the iridium catalyst and B is target proton in the substrate, the optimal conditions for polarization transfer is given as

$$B_{LAC} = |2\pi J_{AA'}/\gamma_H(\delta_A - \delta_B)|, \quad (18)$$

where γ_H – gyromagnetic ratio of protons, δ_A, δ_B – chemical shifts of spins A and B, $J_{AA'}$ – spin–spin coupling constant between A and A′ spins originating from parahydrogen.[139]

Zone 4 is the regime of ultralow field matching conditions (discussed in the previous section) with strong coupling conditions between protons and heteronuclei, also known as the SABRE–SHEATH[143] regime. The polarization transfer can occur between the hydride protons originating from parahydrogen and any heteronuclei of interest in the substrate that is reversibly bound to the iridium complex.[140,141]

3. Applications of parahydrogen in NMR

Parahydrogen in catalysis

Most of the initial applications of PHIP were related to the investigation of organometallic catalysts and homogeneous catalysis (see *e.g.* reviews by Duckett[144,145] and Münnemann *et al.*[146]). In particular, PHIP is one of the most powerful techniques for the *in situ* NMR investigation of hydrogenation reactions and their catalytic mechanisms.[145,147,148] In recent years there is a growing number of studies, where metal-nanoparticles or other heterogeneous catalysts were employed for the generation of PHIP hyperpolarized gases like propene.[38,56,149–172] A major driving force for these developments is the search for the cost-efficient production of hyperpolarized gases for contrast enhancement in medical applications of NMR such as MRI imaging of the lung, as PHIP does not depend on expensive additional hardware and is thus more amenable to implementation in medical diagnostics.[173–175]

In parallel to the applications in MR signal enhancement, PHIP is also an excellent tool for the investigation of the basic hydrogenation mechanisms, and, in the case of homogeneous catalysis also for the investigation of catalytic intermediates.[176] An essential condition for the formation of PHIP is a pair-wise hydrogenation of an unsaturated bond, where both hydrogen atoms stem from the same hydrogen molecule. Owing to this condition, most heterogeneous metal catalysts cannot create PHIP, as the hydrogen molecule dissociates on their surfaces to atomic hydrogen, which migrates on the surface, and hydrogen atoms from different molecules react with the substrate. In order to achieve heterogeneous HET-PHIP by such catalysts, it is necessary to reduce the migration radius by partial poisoning of the surface.[149,153] After such a reduction the spin-coherence

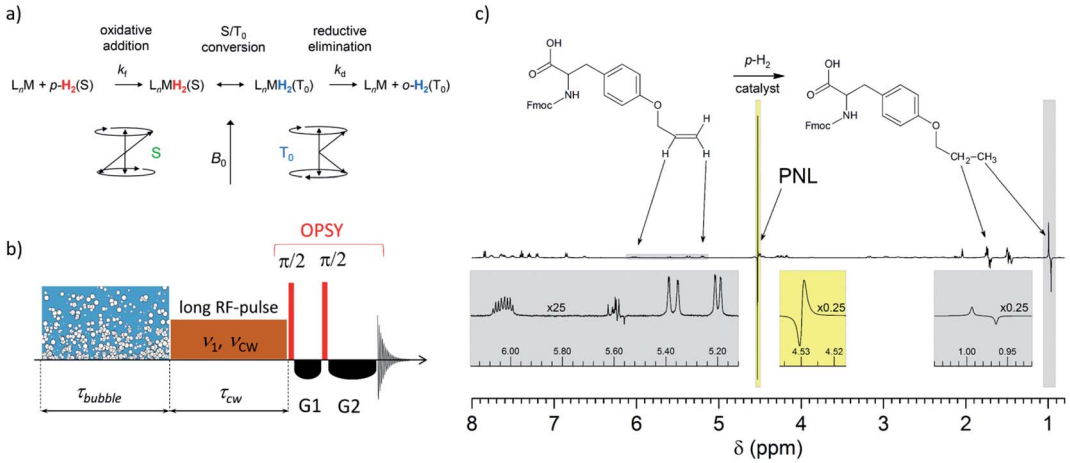

Fig. 10 (a) Magnetic conversion of p-H_2 (spin state S) to o-H_2 in spin state T_0. (b) The PANEL (PArtially NEgative Line) experiment for the indirect detection of the hydrogen catalyst complex. (c) ^{1}H NMR PHIP spectrum recorded during the hydrogenation with *p*-H_2 of Fmoc-*O*-allyl-tyrosine (left) to Fmoc-*O*-propyl-tyrosine (right), showing a strong PNL signal at 4.53 ppm (for details see Kiryutin *et al.*[93]).

between the two hydrogen atoms can be conserved, *e.g.*, by dipolar interactions,[177] and result in a PHIP. An overview about these variants of PHIP was recently published by Pokochueva *et al.*[178]

Ultrasensitive indirect NMR detection of catalytic hydrogen complexes *via* parahydrogen

Kiryutin *et al.*[93] revealed and explained spin exchange processes between molecular hydrogen with two equivalent nuclear spins and transient hydride complexes with two inequivalent hydrogens with different chemical shifts, in which singlet–triplet evolution takes place (see Fig. 10). Spectroscopically, this process is observed as nearly complete overlapping of a negative and a positive line with only slightly different frequencies, leading to a negative component on the low-field part of the absorptive peak of dissolved free hydrogen in solution; hence, it was called Partially Negative Line (PNL) of H_2 in PHIP experiments. The PNL effect was initially found during the investigation of the PHIP enhancement of small oligopeptides. In these experiments, it was found that the ^{1}H NMR signal of

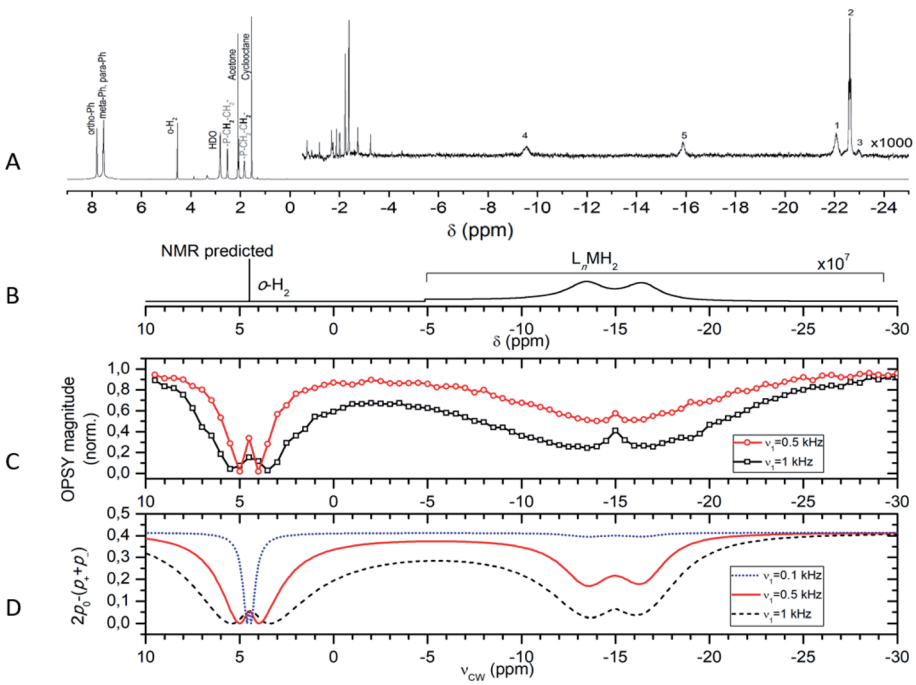

Fig. 11 (A) Thermal 700 MHz ^{1}H NMR spectrum accumulated after bubbling the catalyst solution by *n*-H_2 (512 scans, 30 minutes) and magnification (×1000) of the dihydrogen and dihydride region. Note that there is no signal of any complex between catalyst and hydrogen. (C and D) Experimental and simulated PANEL spectra, showing the signal of the hidden complex (lines at −16.5 ppm and −13.5 ppm). (B) Calculated NMR spectrum of the hidden complex, magnified by factor 10^7 (for details see Kiryutin *et al.*[93]).

dissolved p-H_2 enriched molecular hydrogen exhibits, in the presence of an organometallic hydrogenation catalyst, this unusual PNL-shape. A detailed experimental and theoretical study proved that the PNL results from a strongly enhanced two-spin order, interrelated with selective population of the T_0 level of orthohydrogen (o-H_2). This two-spin order is made visible by a slow asymmetric exchange process between free hydrogen and a transient catalyst–hydrogen complex.

By *Only Parahydrogen Spectroscopy* (OPSY)[179] it was feasible to selectively detect the two-spin order and suppress the signal from thermal o-H_2. It was found that the intensity of the PNL can be strongly affected by cw-like low-power radio frequency (RF) irradiation, resulting in a technique called PANEL (Fig. 10). When the RF-frequency is on resonance with the chemical shift values of one of the hydrogens bound to the elusive catalyst or of the free hydrogen, a strong intensity reduction of the PNL is observed (Fig. 11). Numerical simulations of the experiments performed at 500 and 700 MHz proton frequency showed that the indirect detection has an at least three orders of magnitude higher sensitivity than the normal NMR experiment.

A theoretical model, including reversible binding and S–T_0 evolution, was developed, which reproduces the NMR line-shape, the nutation angle dependence, and the dependence on the frequency of the irradiation field of the PNL, and permits the determination of the proton chemical shift values and the sign of the scalar coupling in the transient NMR-invisible complex, where singlet–triplet conversion takes place. A detailed theoretical analysis of the effect is given in the paper by Kiryutin *et al.*[93]

Understanding and modelling catalytic hydrogenation reactions for PHIP and SABRE

In the continuation of this work, the possibility to utilize non-hyperpolarized Chemical Exchange Saturation Transfer (CEST) NMR in a similar fashion to study short-lived hydride intermediates in the catalytic cycle of an organometallic complex was explored. As example, the SABRE catalyst $[Ir(IMes)(H)_2(Py)_3]^+Cl^-$ was chosen (complex **1** in Fig. 12). In the course of the SABRE formation, transient complexes of the catalyst, the p-H_2 and the substrate (*e.g.*, pyridine) are formed. Understanding the spin dynamics in these complexes is necessary for enhancing the performance of the nuclear spin hyperpolarization technique SABRE. These complexes are low concentrated and undergo reversible ligand exchange with the main complex. They are typically not observable by other NMR techniques.

Knecht *et al.*[180] could show that by eliminating $[Ir(IMes)(H)_2(Py)_3]Cl$ (complex **2** in Fig. 12) and manipulating the spin system by RF-irradiation, the nuclear spin singlet lifetime of the hydride protons can be increased by more than an order of magnitude, from 2.2 ± 0.1 s to 27.2 ± 1.2 s, and the intermediate complexes $[Ir(IMes)(H)_2(Py)_3]$ and $[Ir(CD_3OD)(IMes)(H)_2(Py)_2]$ can be detected, assigned and characterized in solution, *in situ* and at room temperature (see Fig. 12 and Knecht *et al.*[180] for details). Due to its simplicity and ability to unravel unobservable chemical species, the utilized CEST NMR approach has a large application potential for studying short-lived hydride intermediates in catalytic reactions. To model such phenomena, Knecht, Ivanov *et al.*[119] developed techniques for simulating the spin dynamics in the presence of chemical exchange. These techniques allowed them to describe the formation of hyperpolarized o-H_2 and to model quantitatively the PANEL experiment. Employing these techniques, it was possible to describe the polarization formation in SABRE-relay, an extension of the traditional SABRE for polarizing a wider range of substrates by exploiting additional exchange processes

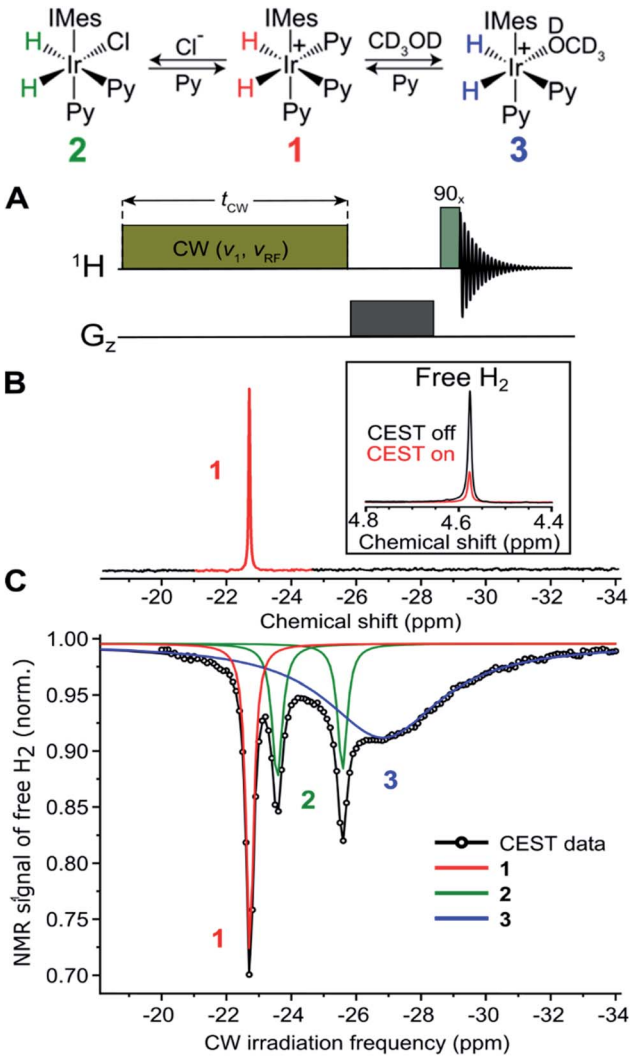

Fig. 12 Upper panel: Molecular diagram of the exchange between the main organometallic complex (SABRE catalyst) $[Ir(IMes)(H)_2(Py)_3]^+Cl^-$ (**1**) and its intermediates **2** and **3** in solution (methanol-d_4). Lower panel: (A) Experimental ^{1}H NMR CEST scheme. Continuous wave (CW) irradiation with an amplitude (ν_1 = 50 Hz) is applied for 3 s at a particular offset frequency ν_{RF} and the integral of the free H_2 signal is recorded; then the offset frequency is incremented, and the experiment is repeated again yielding the CEST spectrum. (B) Standard ^{1}H NMR (500 MHz) spectrum of **1** in methanol-d_4. The inset shows the CEST effect on the free H_2 resonance when saturation is applied to the hydrides of **1** (ν_{RF} = 22.72 ppm). (C) ^{1}H NMR CEST spectrum of **1** in methanol at 280 K showing the presence of dihydride intermediates **2** and **3**. Black: experimental data; red, blue and green lines are Lorentzian fits (for details see Knecht *et al.*[180]).

(see Knecht *et al.*[119] for details). These techniques were later extended to treat highly complex processes with p-H_2, involving several exchange pathways.[181]

In situ gas-phase NMR and para/ortho conversion

In the previous two cases we have observed a magnetic para/ortho-conversion of the parahydrogen in the complex. The p/o conversion can take place *via* various magnetic mechanisms by binding of a single H_2 to a catalytic center or *via* binding of two hydrogen molecules and reorganization of their bonds. In particular, the magnetic conversion mechanism must be distinguished from the chemical conversion by chemical exchange between two hydrogen molecules under the influence of a catalyst. As the chemical process is the analogue of the isotopic scrambling reaction[182]

$$H_2 + D_2 \rightarrow 2HD,$$

In situ gas-phase NMR provides efficient means to probe for chemical conversion mechanisms. It has been shown, that systems catalyzing isotopic scrambling also catalyze the hydrogenation of alkynes and alkenes.[183] Characteristic for these investigations was that the heterogeneous catalyst was in a diamagnetic – or at least – mostly diamagnetic state and could be employed directly inside the NMR magnet by placing it on the bottom or the inner surface of the NMR tube.

Fig. 13 shows two typical examples of this work. In both cases, transition metal nanoparticles (MNPs) stabilized by an organic coating were employed. The first example, taken from Pery *et al.*,[184] displays results obtained for Ru nanoparticles stabilized by hexadecylamine as a protecting ligand. These nanoparticles were investigated by ^{1}H-gas-phase NMR spectroscopy. The MNPs contain adsorbed mobile hydrogen atoms. In order to control the surface hydrogen content, the MNPs were evacuated and exposed to a known hydrogen (H_2) atmosphere. In the next step the H_2 atmosphere is replaced by a D_2 atmosphere, and the conversion of HD on the surface and its desorption are monitored by the appearance of the HD-gas peak at 4.5 ppm (note: HD and H_2 both resonate at 4.5 ppm, but can be distinguished by their line widths, which differ by a factor of *ca.* six[186]). The right panels of Fig. 13 display the results of similar experiments on Ru, Pt and Ru/Pt nanoparticles stabilized with 1,4-bis(diphenylphosphino)butane (dppb) at deuterium pressures of 1 bar and 2 bar.

Potential of PHIP hyperpolarization in heterogeneous catalysis and solid-state NMR

In all cases described above PHIP was always employed for hyperpolarization of fluid (*e.g.*, liquid, or gaseous) samples. Owing to the versatility and cost-efficacy of PHIP based hyperpolarization, an obvious question is, whether PHIP can be employed for the investigation of solid surfaces, similar to the SENS DNP experiment.[187] This would, in contrast to DNP, permit, *e.g.,* the investigation of surface processes on technical catalysts under real world conditions, *e.g.*, at both ambient and elevated temperatures and pressures. This question was theoretically studied by Buntkowsky and Ivanov,[177] who analyzed the spin-dynamics of a heterogeneous catalyzed hydrogenation reaction on the surface of a metal catalyst as a means for creating hyperpolarized surface sites.[177] They assumed that the two hydrogen atoms, stemming from the parahydrogen molecule, are bound as hydrides to different metal centers on a solid surface (Fig. 14). In this case, the *J*-coupling between the protons is small, as compared with dipolar interactions, which have dominant effect on the spin dynamics.

Analytical expressions for the signal enhancement in solid state PHIP NMR spectroscopy employing off-resonant solid state echo detection are developed and tested numerically. Both the analytical calculations and the numerical simulations show clearly that an efficient enhancement of the proton NMR signal in solid state NMR studies of chemisorbed hydrogen on

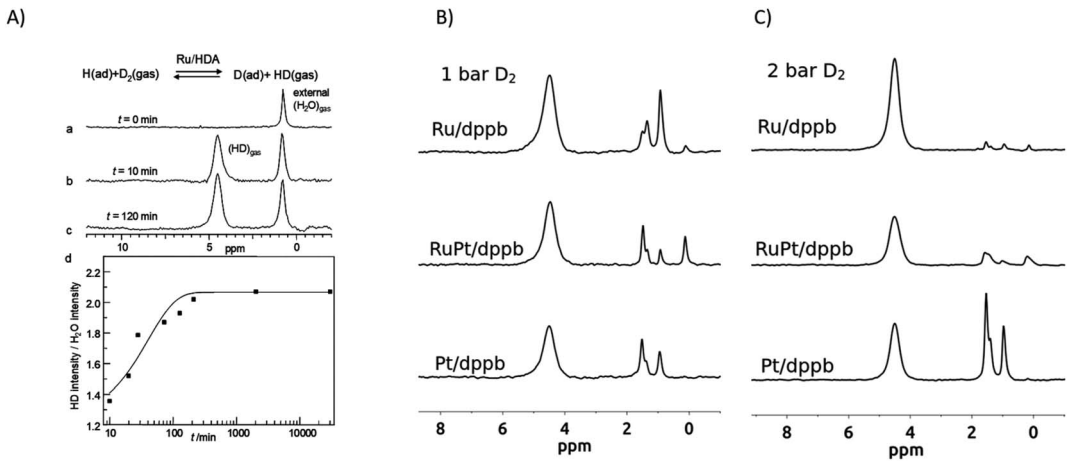

Fig. 13 (A) Upper panel: Gas phase 11.4 Tesla ^{1}H NMR spectra showing the production of HD from the reaction of Ru/hexadecylamine nanoparticles containing adsorbed H with gaseous D_2 in a glass sealed NMR tube (for details see Pery *et al.*[184]). (B and C) Typical ^{1}H gas-phase NMR spectra after exposing solid MNPs at room temperature to 1 bar or 2 bar D_2 gas for 16 h with Ru/dppb, RuPt/dppb and Pt/dppb nanoparticles at two different pressures of D_2 gas. The chemical shift of the HD signal is set to 4.5 ppm (for details see Rothermel *et al.*[185]).

surfaces is possible employing non-resonant solid echo NMR spectroscopy. Assuming a typical reaction efficacy of *ca.* 5%, enhancement-factors of *ca.* 30–40 are expected for two-pulse respectively single pulse experiment, which correspond to three orders of magnitude of sensitivity enhancement. In an extension of work, it was shown that the technique is also applicable in the PASADENA case, where the hydrogenation is performed inside the magnet.[40] This result has important consequences for the practical application of the method, since it allows the design of an *in situ* flow setup, where the para-hydrogen is adsorbed and desorbed from catalyst surfaces inside the NMR magnet.

Application of parahydrogen induced polarization in biochemistry

One of the major application areas of hyperpolarization in general and PHIP in particular is in the field of biochemistry, biophysics, and medical imaging. Characteristic for these applications is the employment of a hyperpolarized marker, which is detected in the NMR spectrometer, respectively the MRI scanner. Such a marker can be a simple noble gas atom like ^{3}He or ^{129}Xe,[188,189] or a small organic molecule, such as hyperpolarized fumarate or a large peptide, like the sunflower-trypsin inhibitor SFTI-1.[190] A very detailed review about the current state of the art of PHIP hyperpolarized metabolites for biological studies with strong emphasis on medical applicability was recently published by Reineri.[80] For this reason the current review focusses on applications related to fumarate, amino acids, peptides and proteins.

PHIP on peptides and amino acids

Owing to the robustness and versatility of solid-phase peptide synthesis (SPPS)[191] on the one hand and the pharmacological importance of peptide based drugs, employing hyperpolarized peptides as markers in magnetic resonance tomography or in biophysical studies on the other hand, PHIP of peptides and amino acids has an immense technical potential.[192] There are several feasible strategies to exploit this potential. Reversible PHIP techniques, like SABRE, can be applied without modifications of native amino acids.[193]

As it is relatively easy to incorporate PHIP markers into peptides, there is a very active research in the field of hyperpolarized amino acids, peptides and small proteins.[50] This interest is driven by the pharmacological importance of peptide based drugs, or their application potential as hyperpolarized peptide markers in biophysical studies or magnetic resonance tomography.

One possible strategy is the chemical modification of amino-acid residues. As an example, Bommerich *et al.*[194,195] employed the acidification of amino acids for *e.g.*, the hyperpolarization of allylglycine or vigabatrin in aqueous solution.

The more versatile and robust pathway to obtain PHIP enhanced NMR of peptides is the insertion of fluorenylmethyloxycarbonyl (fmoc) protected non-natural amino acids with unsaturated PHIP active groups into a peptide *via* SPPS. The unsaturated group can be a dehydrogenized backbone bond,[192,193,196] or an unsaturated side chain, such as an allyl- or alkyne-group.[190,197] The latter approach has the advantage that it imposes smaller restrictions on the conformational freedom of the peptide strand and thus has less influence on the secondary structure of the peptide and its biological function. As the allyl-groups are the hydrogenation product of the propargyl-groups, it is more convenient to employ the latter, as this permits two consecutive hydrogenation reaction steps with the p-H_2: (i) from the triple to the double bond and (ii) from the double bond to the alkyl.

Fmoc-protected propargyl-glycine (Pra) is the smallest non-natural amino acid with an unsaturated side chain. In a systematic study by Koerner et at.,[197] the PHIP activities of a series of Pra-containing tripeptides and two decapeptides were evaluated. They found that the PHIP activity depends strongly on the amino-acid sequence. While peptides like Ala–Pra–Ala, Phe–Pra–Phe or Met–Pra–Met yielded strong signal enhancements, Cys-containing combinations of amino acid residues, such as Cys–Pra–Cys, did not show any measurable PHIP activity. Moreover, even in the PHIP active peptides the obtained enhancement was about an order of magnitude

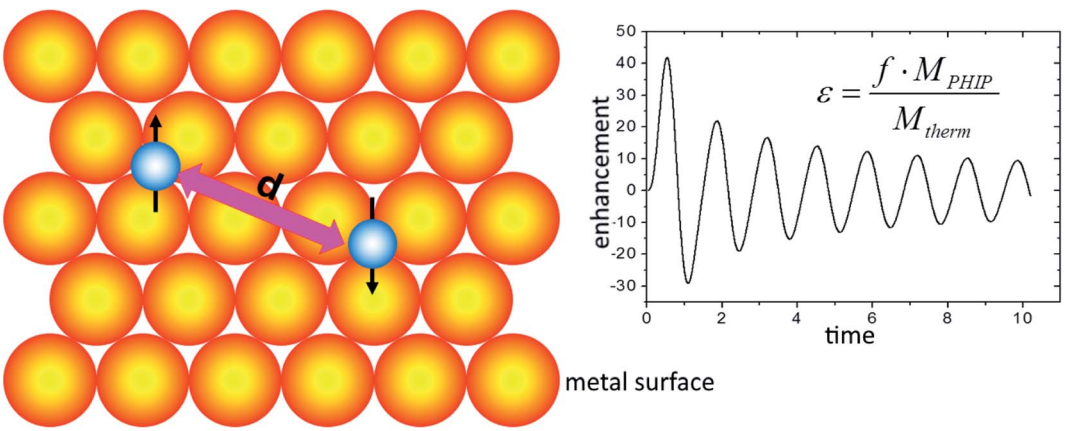

Fig. 14 PHIP on a solid metal surface. Left panel: the magnetic dipolar interaction d couples the two protons from the parahydrogen molecule chemisorbed on the metal surface. Right panel: enhancement as a function of the normalized time $\chi = (d_{zz}t)$ (for details see ref. 177).

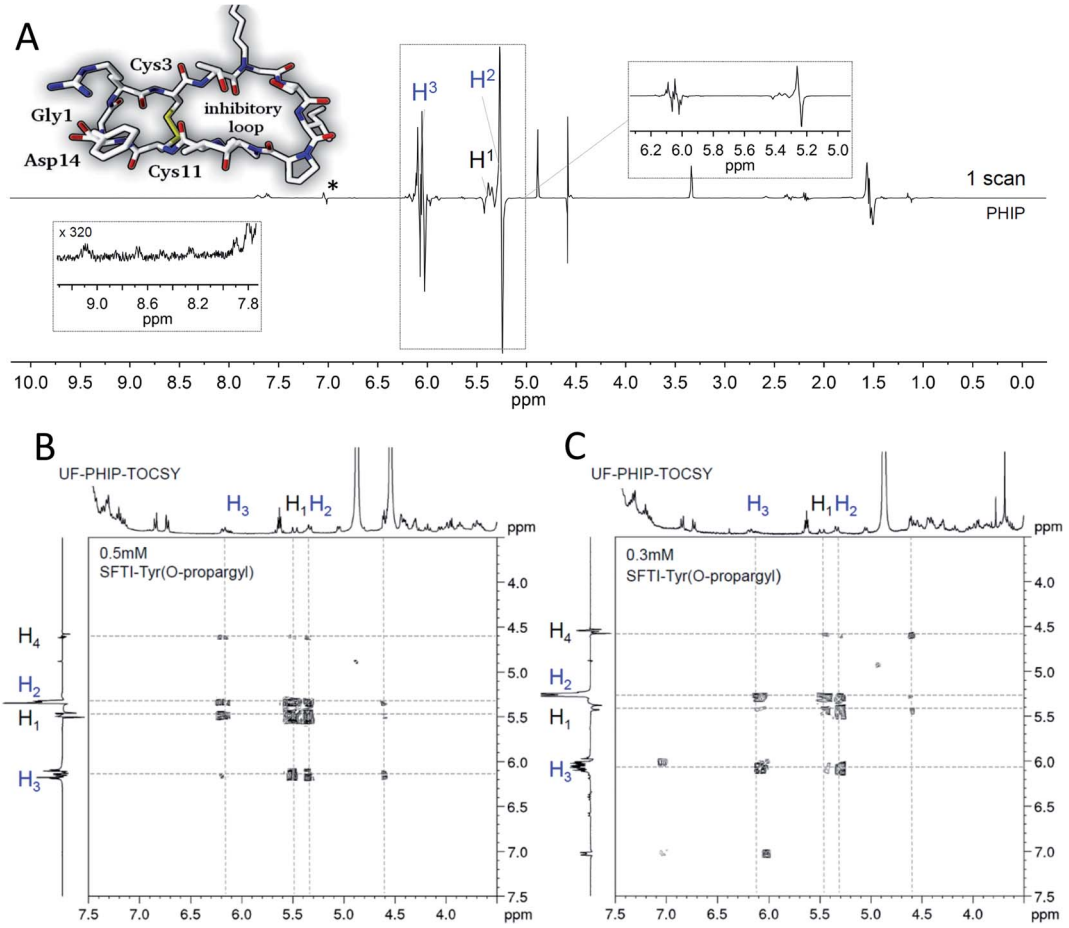

Fig. 15 PHIP enhanced ^{1}H-NMR spectra of a bioactive derivative of the sunflower trypsin inhibitor-1. (A) 1D-NMR (0.96 mM); (B) single scan UF-PHIP-TOCSY (0.5 mM) and 2.5 mM catalyst; (C) single scan UF-PHIP-TOCSY (0.3 mM) and 1.5 mM catalyst. 90% enriched parahydrogen was injected at 3 bars for a period of 10 s. Catalyst = (Rh(dppb)(COD)BF_4), solvent = methanol-d_4. Signal marked with an asterisk (*) is an impurity (for details see Sauer *et al.*[190] and Kiryutin *et al.*[205]).

smaller than the enhancement obtained for neat Pra. In order to achieve higher and more stable enhancements, Sauer *et al.*[190] systematically searched for PHIP-markers suitable for the hyperpolarization of larger peptides, in aqueous solution, *i.e.*, under biocompatible conditions. Employing various tripeptides as test-systems, they could show that an isolated spatial location of the triple bond within the respective label and its accessibility for the hydrogenation catalyst are essential factors for the amount of signal enhancement. As a result of their research, they could show that the labeling of the peptides with *O*-propargyl-L-tyrosine stably yields very strong ^{1}H-NMR signal enhancements.

Fig. 15 shows a typical example application. The label is inserted into a bioactive derivative of the sunflower trypsin inhibitor-1 (SFTI-1), a naturally occurring disulfide-bridged cyclic tetradecapeptide,[198–200] employed as potent inhibitor of serine protease trypsin[200,201] and in tumor diagnostics and treatment.[202,203] Initial ALTADENA type experiments[190] yielded signal enhancement of a factor of 70 for the hyperpolarized protons H^2 and H^3. Under PASADENA conditions, employing an automated setup for PHIP experiments at higher pressures, enhancement factors of about 1200 (Fig. 15A) were achieved.[204] Due to this very high signal enhancement, it was feasible to measure a full 2D-NMR spectrum of the hyperpolarized protons in a single shot,[205] by combining ULTRAFAST[206–212] (UF) 2D-NMR with "out-of-phase echo"[40,213] detection. The example shows the hyperpolarized UF-PHIP-TOCSY spectra obtained after hydrogenation with 90% enriched p-H_2 and 0.5 mM and 0.3 mM solutions (Fig. 15B and C) of hyperpolarized labeled SFTI-1 in a single scan. Despite the low concentration of the hyperpolarized samples, the 2D-NMR spectra including cross-peaks are clearly visible and well resolved. Moreover, as only the hyperpolarized signals are visible, the PHIP enhanced UF-2D-NMR approach provides a very efficient suppression of all thermally polarized background signals. The estimated resulting advantage in measurement time, compared to a standard 2D-TOCSY, is a factor of approximately 180.000.[205] This number clearly demonstrates the potential of PHIP enhanced UF-2D-NMR *e.g.*, to monitor kinetics of low-concentrated peptidic analytes in reactions. The comparison of the thermal and hyperpolarized UF-2D-NMR spectra also shows the intrinsic spectra-editing effect of PHIP. Since only the protons stemming from the parahydrogen and neighboring protons with strong

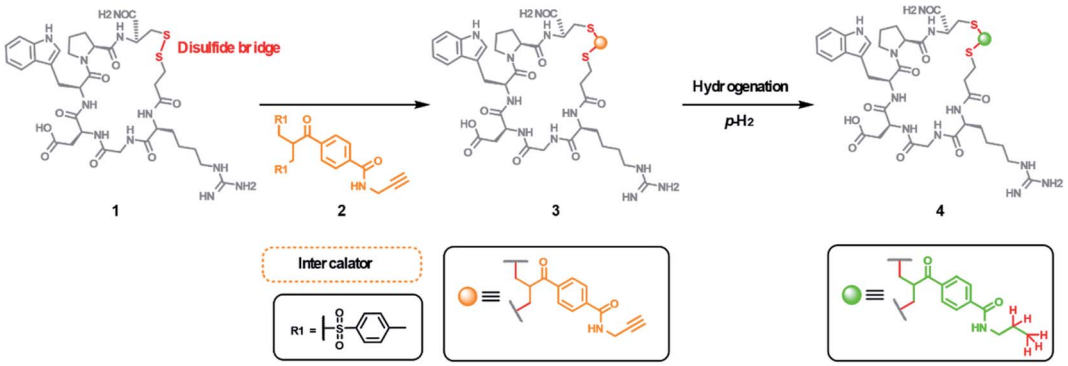

Fig. 16 PHIP labelling of eptifibatide (integrilin, **1**) by insertion of the ethynyl-containing label **2** into the disulfide bridge forms **3**. Hydrogenation of the side-chain alkin-group with p-H_2 yields the hyperpolarized alkyl- (**4**) and allyl- (**4′**) product. Note: for clarity only the final alkyl-product is shown. For details see Fleckenstein *et al.*[214]

scalar couplings are visible, the hyperpolarized spectrum is much simpler than the thermal one.

Fleckenstein *et al.*[214] recently reported a PHIP labelled bioactive derivate of eptifibatide (integrilin), an antiplatelet aggregation inhibitor, which derives from the disintegrin protein barbourin in the venom of certain rattlesnakes. The PHIP-label was synthesized and inserted into the disulfide bridge of eptifibatide *via* reduction of the peptide and insertion by a double Michael addition under physiological conditions (see Fig. 16). This procedure is universally applicable for disulfide-containing biomolecules and preserves their tertiary structure with a minimum of change.

Reversible PHIP techniques like SABRE can be applied without modifications of native amino acids as was shown by Glöggler *et al.*[215] They showed, that non-protected proteinogenic amino acids can be hyperpolarized by SABRE *via* association of the amino- or hydroxy-group to the hydrogenation catalyst, albeit resulting in relatively low polarization levels. Later, Ratajczyk *et al.*[216,217] demonstrated that non-natural amino acid residues containing pyridyl-groups are more efficient labels for SABRE hyperpolarization and can be employed in physiologically relevant substrates, such as the PyFALGEA oligopeptide ligand, which is selective towards the epidermal growth factor receptor (EGFR).

PHIP of metabolites: fumarate as a case example

Fumarate has an immense potential for *in vivo* MRI applications. The hydrogenation of fumarate to malate by the enzyme fumarase is one of the key steps of the Krebs-cycle and thus of interest for monitoring the efficacies of cancer therapies. Employing ^{13}C-DNP hyperpolarization, Gallagher *et al.*[218] could show that malate production from fumarate is increased in treated lymphoma cells and tumors by tumor cell necrosis. Thus, fumarate is an efficient probe to monitor the efficiency of cancer therapies. This seminal discovery started an intense research on the application of hyperpolarized fumarate by MRI.[219–225] Eills and coworkers realized that also PHIP is able to efficiently hyperpolarize fumarate.[226,227] Strong advantages of the PHIP based approach are that the production of the hyperpolarized substrates is faster and scalable with respect to the produced amounts of hyperpolarized molecules, and that the necessary equipment is at least one order of magnitude less expensive than a DNP apparatus and can be easily operated in a clinic environment.

Salient points for the practical application are that: (a) most clinical scanners can monitor only protons; (b) protons are far more sensitive because of their high gyromagnetic ratio and natural abundance; (c) protons permit higher spatial resolution, as they interact stronger with magnetic field gradients than *e.g.*, ^{13}C. Thus, protons are clearly the nuclei of choice for clinical applications. However, there are also a number of challenges in the application of protons, as compared to ^{13}C. The narrow chemical shift dispersion and the large proton background make it difficult to resolve the weak signals of a protonated substrate, and the comparatively short proton T_1 strongly narrows the application time-window of the hyperpolarization. A possible solution to this problem is the application of singlet-state NMR.[137,228–234] When p-H_2 is added to an unsaturated precursor molecule, the protons remain in a nonmagnetic singlet state, as long as they remain chemically and magnetically equivalent. This state is neither directly observable in NMR or MRI, nor addressable by RF pulses. Additionally, the proton singlet state is immune to certain relaxation mechanisms,[36,37] and can have a much longer lifetime. Moreover, singlet-state NMR offers a second advantage, which solves the background problem. Employing the "out of phase echo" (OPE)[213] pulse-sequence with a nonselective 45° or selective 90° detection pulse (OPE-45 or OPE-s90, respectively) and phase-cycles, the background signal of the Zeeman-polarized protons can be suppressed, while only the hyperpolarized molecules are detected. The hyperpolarization can be stored in the singlet state until the molecule undergoes a chemical reaction that renders the protons chemically or magnetically inequivalent. This breaks the proton singlet state, and observable hyperpolarized NMR signals are released.

In the case of fumarate, this effect is created in two steps. In the first step, the hyperpolarized singlet state of fumarate is generated from dicarboxylic acid by hydrogenation with p-H_2. In the second step (see Fig. 17, upper panel), the fumarate is

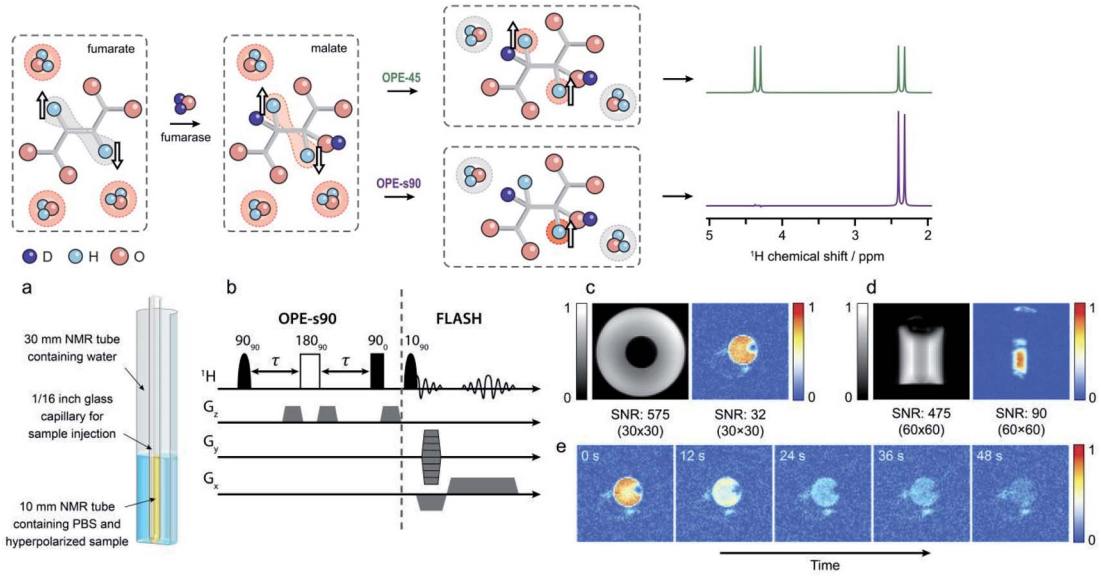

Fig. 17 Upper panel: Sketch of the conversion of hyperpolarized fumarate into malate-D_2, by the fumarase, followed by OPE-45 or OPE-s90 to convert the antiphase proton spin order into in-phase magnetization and suppress water background signals. Lower panel: (a) Imaging phantom. (b) Pulse sequence to acquire hyperpolarized ^{1}H images. (c and d) Comparison between the hyperpolarized and thermal ^{1}H images. For details see Eills *et al.*[63]

converted by fumarase to malate, which breaks the magnetic equivalence of the two hyperpolarized protons and renders them NMR active. In a proof of principle experiment (Fig. 17, lower panel), Eills *et al.*[63] could show that this strategy works indeed by detecting hyperpolarized malate signals of a phantom.

Moreover, fumarate also offers an elegant opportunity to solve the problem of separating the hyperpolarized product from contaminants, such as *e.g.*, residues of the catalyst. The hyperpolarized fumarate can be purified by acid precipitation as a pure solid, and later redissolved at a chosen concentration in a clean aqueous solvent. It was found that it is possible to form hyperpolarized fumarate at several hundred millimolar concentrations, at ^{13}C polarization levels of 30–45% (see Knecht *et al.*[77]). Rodin *et al.*[127] have developed efficient and robust strategies to convert the proton spin order of fumarate into polarization of ^{13}C nuclei. The new pulse sequences exploit adiabatic RF pulses and result in 96% of the maximal theoretically allowed transfer efficiencies. In high-field experiments

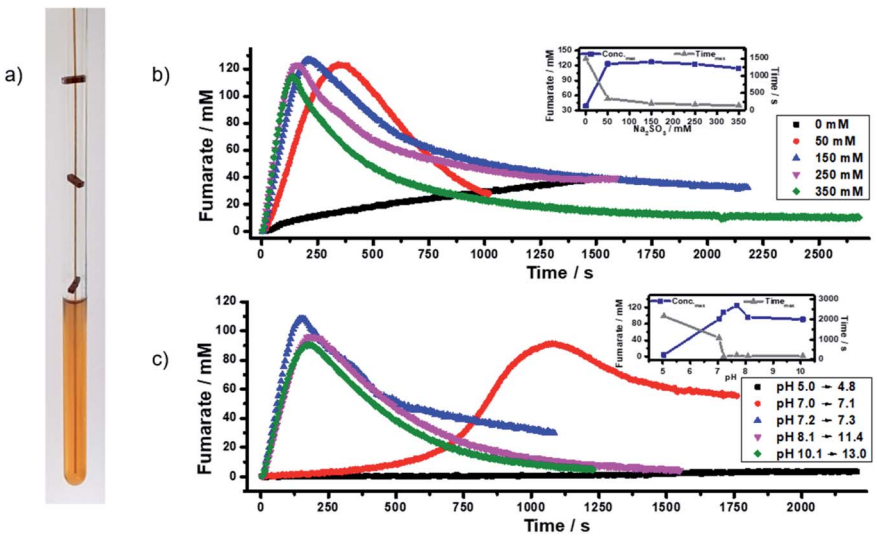

Fig. 18 (a) Photo of the tube with optimized spacers and capillary inside. Influence of (b) sodium sulfite concentration and (c) pH on the formation of fumarate; the inset plots show the maximal fumarate concentration reached and the time it took to reach the maximum. For details see Wienands *et al.*[78]

with p-H_2, this allowed to achieve enhancement factors of the order of 10 000.

Equally important is the optimization of the reaction conditions and the reaction protocol for PHIP of fumarate in water as a physiological medium (Fig. 18). Compared to typical organic solvents, water has a higher viscosity and surface tension and a strong tendency to form bubbles and foams. This problem could be solved by using a glass-capillary which is fixed by spacers inside the NMR tube. In the next step, the dependence of the fumarate production on temperature, pH, and sodium sulfite concentration was determined. Employing these optimized conditions, proton enhancement factors of 3500 at 500 MHz, corresponding to polarizations of $P(^1H) = 28\%$, were obtained (for details see Wienands *et al.*[78]).

4. Outlook and perspectives

With the present review we wanted to demonstrate that parahydrogen-based hyperpolarization techniques have become efficient tools for the sensitivity enhancements of NMR and MRI. With their typical signal enhancement factors of 1000 and above they drastically reduce the time or amount of substance necessary for obtaining high-resolved NMR spectra. In the application area, these signal-enhancements enable the ultra-sensitive detection of catalytic reaction intermediates or the ultra-fast detection of low-concentrated peptides in solution, which would have been completely impossible without them. Moreover, as demonstrated with the fumarate example, it is nowadays feasible to hyperpolarize and clean a biological metabolite, amenable in the future as a marker for the success of cancer therapies.

There are two major factors for this success, namely, on the one-hand the technological advances in the field of reversible and irreversible PHIP and the understanding of the underlying spin-dynamics, and on the other hand the development of efficient transfer complexes, catalysts, and unsaturated substrate precursors. In the field of medical NMR, one can expect the first successful applications of PHIP hyperpolarized substrates, *e.g.*, for the *in vivo* analysis of pharmacokinetics, in the not-too-distant future.

However, also in the field of catalytic studies, parahydrogen has still an immense application potential. PHIP combined with H/D-exchange, solid-state NMR or gas-phase NMR techniques is extremely powerful for the monitoring of heterogeneously catalyzed surface reactions on metal-nanoparticles,[185] and in particular for para/ortho conversion reactions and isotope scrambling.[82,183,235,236]

A further interesting application in the field of PHIP generated hyperpolarization is benchtop NMR.[237,238] Nowadays, there are several commercial vendors, who offer two-channel high-resolution benchtop solution state NMR spectrometers with magnetic fields on the order of 0.9–1.9 Tesla, with very good resolutions well below 1 Hz for protons at prices well below a standard super-conducting high-field NMR spectrometer. As these benchtop spectrometers work cryogen free and are relatively small, they can be easily employed *e.g.*, in an organic preparative lab, under harsh environments or at places, where no cryogens are available. For a detailed overview of their application potential see the recent special issue on compact NMR.[238] The main drawback of these machines is their reduced sensitivity, owing to the low Boltzmann polarization at these low fields. However, combined with parahydrogen based hyperpolarization, these benchtop spectrometers provide highly sensitive solutions.[239–241]

While the PHIP hyperpolarization is conventionally detected by RF-coils, this is not the only possible detection mechanism. In particular at very low fields or for very small sample volumes, where the sensitivity of RF-detection decreases drastically, techniques which directly measure magnetic field strength, such as atomic magnetometers[129,242] or superconducting quantum interference devices (SQUIDs)[243,244] or nitrogen vacancy (NV)[245] based techniques, which have the potential to detect concentration of spins, comparable to a single cell, have strong advantages.

In summary, recent developments of PHIP have paved the way to new applications of magnetic resonance in chemistry, biophysics, and medicine on "real world systems". With further improvements in technology and the physical understanding of the underlying transfer processes, the levels of hyperpolarization will further increase and permit new experiments and diagnostic techniques which were considered impossible a decade ago.

Abbreviations

ALTADENA	Adiabatic longitudinal transport after dissociation engenders net alignment
CASPEr	Cosmic axion spin precession experiment
CEST	Chemical exchange saturation transfer
CIDNP	Chemically induced dynamic nuclear polarization
cw	Continuous wave
DMSO	Dimethyl sulfoxide
DNP	Dynamic nuclear polarization
dppb	1,4-Bis(diphenylphosphino)butane
FC	Field cycling
fmoc	Fluorenylmethyloxycarbonyl
FS	Field sweep
HDA	Hexadecylamine
HET-PHIP	PHIP catalyzed by a heterogeneous catalyst
INEPT	Insensitive nuclei enhancement by polarization transfer
INEPT-SABRE	Combination of INEPT and SABRE
LAC	Level-anti-crossing
LIGHT-SABRE	Low-irradiation generation of high Tesla-SABRE
MNP	Metal nanoparticles
MRI	Magnetic resonance imaging
NHC	N-Heterocyclic carbene
NMR	Nuclear magnetic resonance
NV	Nitrogen vacancy
o-H_2	Orthohydrogen
OPSY	Only parahydrogen spectroscopy

PANEL	Partially negative line experiment
PASADENA	Parahydrogen and synthesis allow dramatically enhanced nuclear alignment
p-H_2	Parahydrogen
PHIP	Parahydrogen induced polarization
PHIP-SAH	PHIP side arm hydrogenation
PHIP-X	PHIP relayed *via* proton exchange
PNL	Partially negative line
Py	Pyridine
RASER	Radiowave amplification by stimulated emission of radiation
RF	Radio frequency
RF-SABRE	SABRE with transfer at high field *via* RF irradiation
SABRE	Signal amplification by reversible exchange
SABRE-SHEATH	SABRE in shield enables alignment transfer to heteronuclei
SENS	Surface enhanced NMR
SEOP	Spin-exchange optical pumping
SFTI-1	sunflower-trypsin inhibitor 1
SLIC-SABRE	Spin lock induced crossing SABRE
SNP	Stimulated nuclear polarization
SPPS	Solid-phase peptide synthesis
SQUID	Superconducting quantum interference devices
TOCSY	Total correlation spectroscopy
UF	Ultrafast
UF-2D-NMR	Ultrafast 2D-NMR

Conflicts of interest

There are no conflicts to declare.

Acknowledgements

Financial support by the German Research Foundation under contracts Bu 911-22-1/2 and Bu 911-29-1 and in the Collaborative Research Centre SFB-1487 “Iron Upgraded” and the Open Access Publishing Fund of Technical University of Darmstadt and by the Ministry of Science and Higher Education of the Russian Federation (Grant No. 075-15-2021-580) is gratefully acknowledged.

References

1 A. W. Overhauser, Polarization of Nuclei in Metals, *Phys. Rev.*, 1953, **92**, 411.
2 T. P. Carver and C. P. Slichter, Polarization of Nuclear Spins in Metals, *Phys. Rev.*, 1953, **92**, 212.
3 T. P. Carver and C. P. Slichter, Experimental Verification of the Overhauser Nuclear Polarization Effect, *Phys. Rev.*, 1956, **102**, 975.
4 A. Abragam and W. G. Proctor, Une novelle méthode de polarization dynamique des noyaux atomiques dans les solides, *C. R. Acad. Sci.*, 1958, **246**, 2253.
5 G. Maier, U. Haeberlen, H. C. Wolf and K. H. Hausser, Optische Kernspin-Polarisation in Anthracen-Kristallen, *Phys. Lett. A*, 1967, **25**, 384–385.
6 K. H. Hausser and D. Stehlik, Dynamic Nuclear Polarization in Liquids, *Adv. Magn. Reson.*, 1968, **3**, 79.
7 D. Stehlik, The Mechanism of Optical Nuclear Polarization, *Excited States*, 1977, **3**, 204–303.
8 W. Happer, E. Miron, S. Schaefer, W. A. Schreiber, W. A. v. Wijngaarden and X. Zeng, Polarization of the nuclear spins of noble-gas atoms by spin exchange with optically pumped alkali-metal atoms, *Phys. Rev. A*, 1984, **29**, 3092.
9 A. Bifone, Y.-Q. Song, R. Seydoux, R. E. Taylor, B. M. Goodson, T. Pietrass, T. F. Budinger, G. Navon and A. Pines, NMR of laser-polarized xenon in human blood, *Proc. Natl. Acad. Sci. U. S. A.*, 1996, **93**, 12932.
10 G. Buntkowsky, W. Hoffmann, T. Kupka, G. Pasterna, M. Jaworska and H. M. Vieth, Application of optical nuclear polarization enhanced C-13 NMR, *J. Phys. Chem. A*, 1998, **102**, 5794–5801.
11 G. Buntkowsky, K. L. Ivanov, H. Zimmermann and H. M. Vieth, Coherent manipulation of non-thermal spin order in optical nuclear polarization experiments, *J. Chem. Phys.*, 2017, **146**, 114501.
12 A. Farkas, *Orthohydrogen, Parahydrogen and Heavy Hydrogen*, Cambridge Univ. Press, Cambridge, 1935.
13 C. R. Bowers and D. P. Weitekamp, Transformation of Symmetrization Order to Nuclear-Spin Magnetization by Chemical Reaction and Nuclear Magnetic Resonance, *Phys. Rev. Lett.*, 1986, **57**, 2645.
14 C. R. Bowers and D. P. Weitekamp, Para-Hydrogen and Synthesis Allow Dramatically Enhanced Nuclear Alignment, *J. Am. Chem. Soc.*, 1987, **109**, 5541–5542.
15 M. G. Pravica and D. P. Weitekamp, Net NMR alignment by adiabatic transport of parahydrogen addition products to high magnetic field, *Chem. Phys. Lett.*, 1988, **145**, 255–258.
16 T. C. Eisenschmidt, R. U. Kirss, P. P. Deutsch, S. I. Hommeltoft, R. Eisenberg, J. Bargon, R. G. Lawler and A. L. Balch, Para hydrogen induced polarization in hydrogenation reactions, *J. Am. Chem. Soc.*, 1987, **109**, 8089–8091.
17 R. W. Adams, J. A. Aguilar, K. D. Atkinson, M. J. Cowley, P. I. P. Elliott, S. B. Duckett, G. G. R. Green, I. G. Khazal, J. López-Serrano and D. C. Williamson, Reversible Interactions with para-Hydrogen Enhance NMR Sensitivity by Polarization Transfer, *Science*, 2009, **323**, 1708–1711.
18 L. S. Lloyd, R. W. Adams, M. Bernstein, S. Coombes, S. B. Duckett, G. G. Green, R. J. Lewis, R. E. Mewis and C. J. Sleigh, Utilization of SABRE-derived hyperpolarization to detect low-concentration analytes *via* 1D and 2D NMR methods, *J. Am. Chem. Soc.*, 2012, **134**, 12904–12907.
19 V. Daniele, F.-X. Legrand, P. Berthault, J.-N. Dumez and G. Huber, Single-Scan Multidimensional NMR Analysis of Mixtures at Sub-Millimolar Concentrations by using SABRE Hyperpolarization, *ChemPhysChem*, 2015, **16**, 3413–3417.
20 R. E. Wasylishen, *Handbook of high field dynamic nuclear polarization*, Wiley, Chichester, 2020.

21 A. B. Schmidt, C. R. Bowers, K. Buckenmaier, E. Y. Chekmenev, H. de Maissin, J. Eills, F. Ellermann, S. Glöggler, J. W. Gordon, S. Knecht, I. V. Koptyug, J. Kuhn, A. N. Pravdivtsev, F. Reineri, T. Theis, K. Them and J.-B. Hövener, Instrumentation for Hydrogenative Parahydrogen-Based Hyperpolarization Techniques, *Anal. Chem.*, 2022, **94**, 479–502.

22 S. B. Duckett, C. L. Newell and R. Eisenberg, Observation of New Intermediates in Hydrogenation Catalyzed by Wilkinsons Catalyst, Rhcl(Pph(3))(3), Using Parahydrogen-Induced Polarization, *J. Am. Chem. Soc.*, 1994, **116**, 10548–10556.

23 S. B. Duckett and C. J. Sleigh, Applications of the parahydrogen phenomenon: A chemical perspective, *Prog. Nucl. Magn. Reson. Spectrosc.*, 1999, **34**, 71–92.

24 S. M. Oldham, J. F. Houlis, C. J. Sleigh, S. B. Duckett and R. Eisenberg, Observation of new intermediates in the reaction of dihydrogen with iridium, rhodium, and mixed metal A-frame complexes with parahydrogen-induced polarization, *Organometallics*, 2000, **19**, 2985–2993.

25 S. B. Duckett and D. Blazina, The study of inorganic systems by NMR spectroscopy in conjunction with parahydrogen-induced polarisation, *Eur. J. Inorg. Chem.*, 2003, 2901–2912.

26 S. B. Duckett and R. E. Mewis, Application of Parahydrogen Induced Polarization Techniques in NMR Spectroscopy and Imaging, *Acc. Chem. Res.*, 2012, **45**, 1247–1257.

27 B. Heaton, *Mechanisms in homogeneous catalysis: a spectroscopic approach*, VCH Verlagsgesellschaft mbH, 2005.

28 J. Bargon, in *Handbook of homogeneous hydrogenation*, Elsevier, 2007.

29 S. B. Duckett and N. J. Wood, Parahydrogen-based NMR methods as a mechanistic probe in inorganic chemistry, *Coord. Chem. Rev.*, 2008, **252**, 2278–2291.

30 C. B. LeMaster, Nuclear magnetic resonance spectroscopy of molecules in the gas phase, *Prog. Nucl. Magn. Reson. Spectrosc.*, 1997, **31**, 119–154.

31 B. D. Ross and N. S. True, NMR spectroscopy of cyclohexane. Gas-phase conformational kinetics, *J. Am. Chem. Soc.*, 1983, **105**, 4871–4875.

32 P. M. Kating, P. J. Krusic, D. C. Roe and B. E. Smart, Hydrogenation of Fluoroolefins Studied by Gas Phase NMR: A New Technique for Heterogeneous Catalysis, *J. Am. Chem. Soc.*, 1996, **118**, 10000–10001.

33 F. Rittig, D. J. Aurentz, C. G. Coe, R. J. Kitzhoffer and J. M. Zielinski, Pure- and Mixed-Gas Sorption Measurements on Zeolitic Adsorbents *via* Gas-Phase Nuclear Magnetic Resonance, *Ind. Eng. Chem. Res.*, 2002, **41**, 4430–4434.

34 A. Adamczyk, Y. Xu, B. Walaszek, F. Roelofs, T. Pery, K. Pelzer, K. Philippot, B. Chaudret, H.-H. Limbach, H. Breitzke and G. Buntkowsky, Solid State and Gas Phase NMR Studies of Immobilized Catalysts and Catalytic Active Nanoparticles, *Top. Catal.*, 2008, **48**, 75–83.

35 A. Bordet, L.-M. Lacroix, K. Soulantica and B. Chaudret, A New Approach to the Mechanism of Fischer-Tropsch Syntheses Arising from Gas Phase NMR and Mass Spectrometry, *ChemCatChem*, 2016, **8**, 1727–1731.

36 L. S. Bouchard, S. R. Burt, M. S. Anwar, K. V. Kovtunov, I. V. Koptyug and A. Pines, NMR imaging of catalytic hydrogenation in microreactors with the use of para-hydrogen, *Science*, 2008, **319**, 442–445.

37 A. A. Lysova and I. V. Koptyug, Magnetic resonance imaging methods for *in situ* studies in heterogeneous catalysis, *Chem. Soc. Rev.*, 2010, **39**, 4585–4601.

38 L.-S. Bouchard, K. V. Kovtunov, S. R. Burt, M. S. Anwar, I. V. Koptyug, R. Z. Sagdeev and A. Pines, Para-Hydrogen-Enhanced Hyperpolarized Gas-Phase Magnetic Resonance Imaging, *Angew. Chem., Int. Ed.*, 2007, **46**, 4064–4068.

39 J. F. Dechent, L. Buljubasich, L. M. Schreiber, H. W. Spiess and K. Münnemann, Proton magnetic Resonance Imaging with para-hydrogen induced polarization, *Phys. Chem. Chem. Phys.*, 2012, **14**, 2346–2352.

40 T. Ratajczyk, T. Gutmann, S. Dillenberger, S. Abdulhussaein, J. Frydel, H. Breitzke, U. Bommerich, T. Trantzschel, J. Bernarding, P. C. M. M. Magusin and G. Buntkowsky, Time domain parahydrogen induced polarization, *Solid State Nucl. Magn. Reson.*, 2012, **43–44**, 14–21.

41 K. L. Ivanov, A. V. Yurkovskaya and H. M. Vieth, Coherent transfer of hyperpolarization in coupled spin systems at variable magnetic field, *J. Chem. Phys.*, 2008, **128**, 154701.

42 S. E. Korchak, K. L. Ivanov, A. V. Yurkovskaya and H. M. Vieth, Para-hydrogen induced polarization in multi-spin systems studied at variable magnetic field, *Phys. Chem. Chem. Phys.*, 2009, **11**, 11146–11156.

43 Q. Gong, A. Gordji-Nejad, B. Blümich and S. Appelt, Trace Analysis by Low-Field NMR: Breaking the Sensitivity Limit, *Anal. Chem.*, 2010, **11**, 7078–7082.

44 S. Appelt, S. Glöggler, F. W. Häsing, U. Sieling, A. G. Nejad and B. Blümich, NMR spectroscopy in the milli-Tesla regime: Measurement of 1H chemical-shift differences below the line width, *Chem. Phys. Lett.*, 2010, **485**, 217–220.

45 S. Glöggler, M. Emondts, J. Colell, R. Müller, B. Blümich and S. Appelt, Selective drug trace detection with low-field NMR, *Analyst*, 2011, **136**, 1566–1568.

46 J. Natterer and J. Bargon, Parahydrogen induced polarization, *Prog. Nucl. Magn. Reson. Spectrosc.*, 1997, **31**, 293–315.

47 R. A. Green, R. W. Adams, S. B. Duckett, R. E. Mewis, D. C. Williamson and G. G. R. Green, The theory and practice of hyperpolarization in magnetic resonance using parahydrogen, *Prog. Nucl. Magn. Reson. Spectrosc.*, 2012, **67**, 1–48.

48 M. H. Levitt, *Annu. Rev. Phys. Chem.*, 2012, **63**, 89–105.

49 G. Buntkowsky and H. H. Limbach, in *Hydrogen-Transfer Reactions*, ed. J. P. Hynes, J. P. Klinman, H. H. Limbach and R. L. Schowen, Wiley-VCH, Weinheim, 2006, pp. 639–682.

50 A. N. Pravdivtsev, G. Buntkowsky, S. B. Duckett, I. V. Koptyug and J.-B. Hövener, Parahydrogen-Induced Polarization of Amino Acids, *Angew. Chem., Int. Ed.*, 2021, **60**, 23496–23507.

51 P. J. Rayner, M. J. Burns, A. M. Olaru, P. Norcott, M. Fekete, G. G. R. Green, L. A. R. Highton, R. E. Mewis and S. B. Duckett, Delivering strong 1H nuclear hyperpolarization levels and long magnetic lifetimes through signal amplification by reversible exchange, *Proc. Natl. Acad. Sci. U. S. A.*, 2017, **114**, E3188–E3194.

52 K. Münnemann, M. Kölzer, I. Blakey, A. K. Whittaker and K. J. Thurecht, Hyperbranched polymers for molecular imaging: designing polymers for parahydrogen induced polarisation (PHIP), *Chem. Commun.*, 2012, **48**, 1583–1585.

53 T. Trantzschel, J. Bernarding, M. Plaumann, D. Lego, T. Gutmann, T. Ratajczyk, S. Dillenberger, G. Buntkowsky, J. Bargon and U. Bommerich, Parahydrogen induced polarization in face of keto-enol tautomerism: proof of concept with hyperpolarized ethanol, *Phys. Chem. Chem. Phys.*, 2012, **14**, 5601–5604.

54 K. Them, F. Ellermann, A. N. Pravdivtsev, O. G. Salnikov, I. V. Skovpin, I. V. Koptyug, R. Herges and J.-B. Hövener, Parahydrogen-Induced Polarization Relayed *via* Proton Exchange, *J. Am. Chem. Soc.*, 2021, **143**, 13694–13700.

55 I. V. Skovpin, V. V. Zhivonitko, R. Kaptein and I. V. Koptyug, Generating Parahydrogen-Induced Polarization Using Immobilized Iridium Complexes in the Gas-Phase Hydrogenation of Carbon–Carbon Double and Triple Bonds, *Appl. Magn. Reson.*, 2013, **44**, 289–300.

56 R. Sharma and L.-S. Bouchard, Strongly hyperpolarized gas from parahydrogen by rational design of ligand-capped nanoparticles, *Sci. Rep.*, 2012, **2**, 277.

57 S. Hadjiali, R. Savka, M. Plaumann, U. Bommerich, S. Bothe, T. Gutmann, T. Ratajczyk, J. Bernarding, H.-H. Limbach, H. Plenio and G. Buntkowsky, Substituent Influences on the NMR Signal Amplification of Ir Complexes with Heterocyclic Carbene Ligands, *Appl. Magn. Reson.*, 2019, **50**, 895–902.

58 S. Hadjiali, M. Bergmann, A. Kiryutin, S. Knecht, G. Sauer, M. Plaumann, H.-H. Limbach, H. Plenio and G. Buntkowsky, The application of novel Ir-NHC polarization transfer complexes by SABRE, *J. Chem. Phys.*, 2019, **151**, 244201.

59 I. V. Koptyug, K. V. Kovtunov, S. R. Burt, M. S. Anwar, C. Hilty, S.-I. Han, A. Pines and R. Z. Sagdeev, para-Hydrogen-induced polarization in heterogeneous hydrogenation reactions, *J. Am. Chem. Soc.*, 2007, **129**, 5580–5586.

60 M. Srour, S. Hadjiali, K. Brunnengräber, H. Weidler, Y. Xu, H. Breitzke, T. Gutmann and G. Buntkowsky, A Novel Wilkinson's Type Silica Supported Polymer Catalyst: Insights from Solid-State NMR and Hyperpolarization Techniques, *J. Phys. Chem. C*, 2021, **125**, 7178–7187.

61 M. Srour, S. Hadjiali, G. Sauer, K. Brunnengräber, H. Breitzke, Y. Xu, H. Weidler, H.-H. Limbach, T. Gutmann and G. Buntkowsky, Synthesis and Solid-State NMR Characterization of a Robust, Pyridyl-Based Immobilized Wilkinson's Type Catalyst with High Catalytic Performance, *ChemCatChem*, 2016, **8**, 3409–3416.

62 S. Abdulhussain, H. Breitzke, T. Ratajczyk, A. Grünberg, M. Srour, D. Arnaut, H. Weidler, U. Kunz, H. J. Kleebe, U. Bommerich, J. Bernarding, T. Gutmann and G. Buntkowsky, Synthesis, solid-state NMR characterization, and application for hydrogenation reactions of a novel Wilkinson's-type immobilized catalyst, *Chemistry*, 2014, **20**, 1159–1166.

63 J. Eills, E. Cavallari, R. Kircher, G. Di Matteo, C. Carrera, L. Dagys, M. H. Levitt, K. L. Ivanov, S. Aime, F. Reineri, K. Münnemann, D. Budker, G. Buntkowsky and S. Knecht, Singlet-Contrast Magnetic Resonance Imaging: Unlocking Hyperpolarization with Metabolism, *Angew. Chem., Int. Ed.*, 2021, **60**, 6791–6798.

64 T. Gutmann, T. Ratajczyk, Y. Xu, H. Breitzke, A. Grünberg, S. Dillenberger, U. Bommerich, T. Trantzschel, J. Bernarding and G. Buntkowsky, Understanding the leaching properties of heterogenized catalysts: a combined solid-state and PHIP NMR study, *Solid State Nucl. Magn. Reson.*, 2010, **38**, 90–96.

65 T. Gutmann, T. Ratajczyk, S. Dillenberger, Y. Xu, A. Grünberg, H. Breitzke, U. Bommerich, T. Trantzschel, J. Bernarding and G. Buntkowsky, New investigations of technical rhodium and iridium catalysts in homogeneous phase employing para-hydrogen induced polarization, *Solid State Nucl. Magn. Reson.*, 2011, **40**, 88–90.

66 S. Appelt, A. Kentner, S. Lehmkuhl and B. Blümich, From LASER physics to the para-hydrogen pumped RASER, *Prog. Nucl. Magn. Reson. Spectrosc.*, 2019, **114–115**, 1–32.

67 M. Suefke, S. Lehmkuhl, A. Liebisch, B. Blümich and S. Appelt, Para-hydrogen raser delivers sub-millihertz resolution in nuclear magnetic resonance, *Nat. Phys.*, 2017, **13**, 568–572.

68 D. Budker, P. W. Graham, M. Ledbetter, S. Rajendran and A. O. Sushkov, Proposal for a Cosmic Axion Spin Precession Experiment (CASPEr), *Phys. Rev. X*, 2014, **4**, 021030.

69 A. Garcon, J. W. Blanchard, G. P. Centers, N. L. Figueroa, P. W. Graham, D. F. Jackson Kimball, S. Rajendran, A. O. Sushkov, Y. V. Stadnik, A. Wickenbrock, T. Wu and D. Budker, Constraints on bosonic dark matter from ultralow-field nuclear magnetic resonance, *Sci. Adv.*, 2019, **5**, eaax4539.

70 K. Golman, O. Axelsson, H. Johannesson, S. Mansson, C. Olofsson and J. S. Petersson, Parahydrogen-induced polarization in imaging: Subsecond C-13 angiography, *Magn. Reson. Med.*, 2001, **46**, 1–5.

71 H. Jóhannesson, O. Axelsson and M. Karlsson, Transfer of para-hydrogen spin order into polarization by diabatic field cycling, *C. R. Phys.*, 2004, **5**, 315–324.

72 L. E. Olsson, C. M. Chai, O. Axelsson, M. Karlsson, K. Golman and J. S. Petersson, MR coronary angiography in pigs with intraarterial injections of a hyperpolarized ^{13}C substance, *Magn. Reson. Med.*, 2006, **55**, 731–737.

73 E. Y. Chekmenev, J. Hövener, V. A. Norton, K. Harris, L. S. Batchelder, P. Bhattacharya, B. D. Ross and D. P. Weitekamp, PASADENA hyperpolarization of succinic acid for MRI and NMR spectroscopy, *J. Am. Chem. Soc.*, 2008, **130**, 4212–4213.

74 E. Terreno, D. D. Castelli, A. Viale and S. Aime, Challenges for molecular magnetic resonance imaging, *Chem. Rev.*, 2010, **110**, 3019–3042.

75 U. Bommerich, T. Trantzschel, S. Mulla-Osman, G. Buntkowsky, J. Bargon and J. Bernarding, Hyperpolarized 19F-MRI: parahydrogen induced polarization and field variation enabling 19F-MRI at low spin density, *Phys. Chem. Chem. Phys.*, 2010, **12**, 10309–10312.

76 A. B. Schmidt, S. Berner, M. Braig, M. Zimmermann, J. Hennig, D. von Elverfeldt and J.-B. Hövener, *In vivo* ^{13}C-MRI using SAMBADENA, *PLoS One*, 2018, **13**, e0200141.

77 S. Knecht, J. W. Blanchard, D. Barskiy, E. Cavallari, L. Dagys, E. van Dyke, M. Tsukanov, B. Bliemel, K. Münnemann, S. Aime, F. Reineri, M. H. Levitt, G. Buntkowsky, A. Pines, P. Blümler, D. Budker and J. Eills, Rapid hyperpolarization and purification of the metabolite fumarate in aqueous solution, *Proc. Natl. Acad. Sci. U. S. A.*, 2021, **118**, e2025383118.

78 L. Wienands, F. Theiß, J. Eills, L. Rösler, S. Knecht and G. Buntkowsky, Optimizing the Reaction Conditions for the Formation of Fumarate *via* Trans-Hydrogenation, *Appl. Magn. Reson.*, 2021, **53**, 615–634.

79 J.-B. Hövener, A. N. Pravdivtsev, B. Kidd, C. R. Bowers, S. Glöggler, K. V. Kovtunov, M. Plaumann, R. Katz-Brull, K. Buckenmaier and A. Jerschow, Parahydrogen-based hyperpolarization for biomedicine, *Angew. Chem., Int. Ed.*, 2018, **57**, 11140–11162.

80 F. Reineri, E. Cavallari, C. Carrera and S. Aime, Hydrogenative-PHIP polarized metabolites for biological studies, *Magma*, 2021, **34**, 25–47.

81 S. Aime, W. Dastru, R. Gobetto, D. Santelia and A. Viale, Agents for polarization enhancement in MRI, *Mol. Imaging*, 2008, 247–272.

82 G. Buntkowsky, B. Walaszek, A. Adamczyk, Y. Xu, H. H. Limbach and B. Chaudret, Mechanism of nuclear spin initiated para-H-2 to ortho-H-2 conversion, *Phys. Chem. Chem. Phys.*, 2006, **8**, 1929–1935.

83 S. Wagner, Conversion rate of para-hydrogen to ortho-hydrogen by oxygen: implications for PHIP gas storage and utilization, *Magma*, 2014, **27**, 195–199.

84 C. R. Bowers and D. P. Weitekamp, Parahydrogen and synthesis allow dramatically enhanced nuclear alignment, *J. Am. Chem. Soc.*, 1987, **109**, 5541–5542.

85 G. Buntkowsky, J. Bargon and H.-H. Limbach, A Dynamic Model of Reaction Pathway Effects on Parahydrogen-Induced Nuclear Spin Polarization, *J. Am. Chem. Soc.*, 1996, **118**, 8677–8683.

86 C. R. Bowers, D. H. Jones, R. Kurur, J. A. Labinger, M. G. Pravica and D. P. Weitekamp, Symmetrization Postulate and Nuclear Magnetic Resonance of Reacting Systems, *Adv. Magn. Reson.*, 1990, **14**, 269–291.

87 D. Canet, C. Aroulanda, P. Mutzenhardt, S. Aime, R. Gobetto and F. Reineri, Para-hydrogen enrichment and hyperpolarization, *Concepts Magn. Reson., Part A*, 2006, **28**, 321–330.

88 K. L. Ivanov, A. Wagenpfahl, C. Deibel and J. Matysik, Spin-chemistry concepts for spintronics scientists, *Beilstein J. Nanotechnol.*, 2017, **8**, 1427–1445.

89 K. L. Ivanov, A. V. Yurkovskya, N. N. Fishman, A. S. Kiryutin, R. Z. Sagdeev and H.-M. Vieth, Chemically Induced Spin Hyperpolarization: Coherence Formation in Reaction Products, *Appl. Magn. Reson.*, 2021, **53**, 595–613.

90 O. B. Morozova and K. L. Ivanov, Time-Resolved Chemically Induced Dynamic Nuclear Polarization of Biologically Important Molecules, *ChemPhysChem*, 2019, **20**, 197–215.

91 O. B. Morozova, A. V. Yurkovskaya, H.-M. Vieth, D. V. Sosnovsky and K. L. Ivanov, Light-induced spin hyperpolarisation in condensed phase, *Mol. Phys.*, 2017, **115**, 2907–2943.

92 D. A. Markelov, V. P. Kozinenko, S. Knecht, A. S. Kiryutin, A. V. Yurkovskaya and K. L. Ivanov, Singlet to triplet conversion in molecular hydrogen and its role in parahydrogen induced polarization, *Phys. Chem. Chem. Phys.*, 2021, **23**, 20936–20944.

93 A. S. Kiryutin, G. Sauer, A. V. Yurkovskaya, H.-H. Limbach, K. L. Ivanov and G. Buntkowsky, Parahydrogen Allows Ultrasensitive Indirect NMR Detection of Catalytic Hydrogen Complexes, *J. Phys. Chem. C*, 2017, **121**, 9879–9888.

94 A. Brinkmann, Introduction to average Hamiltonian theory. I. Basics, *Concepts Magn. Reson., Part A*, 2016, **45**, e21414.

95 K. V. Kovtunov, E. V. Pokochueva, O. G. Salnikov, S. F. Cousin, D. Kurzbach, B. Vuichoud, S. Jannin, E. Y. Chekmenev, B. M. Goodson, D. A. Barskiy and I. V. Koptyug, Hyperpolarized NMR Spectroscopy: d-DNP, PHIP, and SABRE Techniques, *Chem.–Asian J.*, 2018, **13**, 1857–1871.

96 K. L. Ivanov, A. V. Yurkovskaya and H.-M. Vieth, Parahydrogen Induced Polarization in Scalar Coupled Systems: Analytical Solutions for Spectral Patterns and their Field Dependence, *Z. Phys. Chem.*, 2012, **226**, 1315–1342.

97 A. S. Kiryutin, K. L. Ivanov, A. V. Yurkovskaya, R. Kaptein and H.-M. Vieth, Transfer of Parahydrogen Induced Polarization in Scalar Coupled Systems at Variable Magnetic Field, *Z. Phys. Chem.*, 2012, **226**, 1343–1362.

98 S. B. Duckett, C. L. Newell and R. Eisenberg, More than INEPT: parahydrogen and INEPT + give unprecedented resonance enhancement to carbon-13 by direct proton polarization transfer, *J. Am. Chem. Soc.*, 1993, **115**, 1156–1157.

99 J. Barkemeyer, M. Haake and J. Bargon, Hetero-NMR Enhancement *via* Parahydrogen Labeling, *J. Am. Chem. Soc.*, 1995, **117**, 2927–2928.

100 L. T. Kuhn and J. Bargon, in *In situ NMR Methods in Catalysis*, ed. J. Bargon and L. T. Kuhn, Springer Berlin Heidelberg, Berlin, Heidelberg, 2007, pp. 25–68.

101 M. Plaumann, U. Bommerich, T. Trantzschel, D. Lego, S. Dillenberger, G. Sauer, J. Bargon, G. Buntkowsky and J. Bernarding, Parahydrogen-induced polarization transfer to 19F in perfluorocarbons for 19F NMR spectroscopy and MRI, *Chemistry*, 2013, **19**, 6334–6339.

102 K. Buckenmaier, M. Rudolph, C. Back, T. Misztal, U. Bommerich, P. Fehling, D. Koelle, R. Kleiner, H. A. Mayer, K. Scheffler, J. Bernarding and M. Plaumann, SQUID-based detection of ultra-low-field multinuclear NMR of substances hyperpolarized using signal amplification by reversible exchange, *Sci. Rep.*, 2017, **7**, 13431.

103 S. Korchak, S. Yang, S. Mamone and S. Glöggler, Pulsed Magnetic Resonance to Signal-Enhance Metabolites within Seconds by utilizing para-Hydrogen, *ChemistryOpen*, 2018, **7**, 344–348.

104 S. Korchak, S. Mamone and S. Glöggler, Over 50% ^{1}H and ^{13}C Polarization for Generating Hyperpolarized Metabolites—A para-Hydrogen Approach, *ChemistryOpen*, 2018, **7**, 672–676.

105 S. Lehmkuhl, M. Suefke, A. Kentner, Y.-F. Yen, B. Blümich, M. S. Rosen, S. Appelt and T. Theis, SABRE polarized low field rare-spin spectroscopy, *J. Chem. Phys.*, 2020, **152**, 184202.

106 V. P. Kozinenko, A. S. Kiryutin, A. V. Yurkovskaya and K. L. Ivanov, Polarization of low-γ nuclei by transferring spin order of parahydrogen at high magnetic fields, *J. Magn. Reson.*, 2019, **309**, 106594.

107 A. N. Pravdivtsev, A. V. Yurkovskaya, N. N. Lukzen, K. L. Ivanov and H.-M. Vieth, Highly Efficient Polarization of Spin-1/2 Insensitive NMR Nuclei by Adiabatic Passage through Level Anticrossings, *J. Phys. Chem. Lett.*, 2014, **5**, 3421–3426.

108 A. N. Pravdivtsev, A. V. Yurkovskaya, H. Zimmermann, H.-M. Vieth and K. L. Ivanov, Transfer of SABRE-derived hyperpolarization to spin-1/2 heteronuclei, *RSC Adv.*, 2015, **5**, 63615–63623.

109 A. N. Pravdivtsev, A. V. Yurkovskaya, N. N. Lukzen, H.-M. Vieth and K. L. Ivanov, Exploiting level anti-crossings (LACs) in the rotating frame for transferring spin hyperpolarization, *Phys. Chem. Chem. Phys.*, 2014, **16**, 18707–18719.

110 F. Reineri, T. Boi and S. Aime, Parahydrogen induced polarization of 13 C carboxylate resonance in acetate and pyruvate, *Nat. Commun.*, 2015, **6**, 5858.

111 N. V. Chukanov, O. G. Salnikov, R. V. Shchepin, K. V. Kovtunov, I. V. Koptyug and E. Y. Chekmenev, Synthesis of Unsaturated Precursors for Parahydrogen-Induced Polarization and Molecular Imaging of 1-^{13}C-Acetates and 1-^{13}C-Pyruvates *via* Side Arm Hydrogenation, *ACS Omega*, 2018, **3**, 6673–6682.

112 E. Cavallari, C. Carrera, M. Sorge, G. Bonne, A. Muchir, S. Aime and F. Reineri, The 13 C hyperpolarized pyruvate generated by ParaHydrogen detects the response of the heart to altered metabolism in real time, *Sci. Rep.*, 2018, **8**, 8366.

113 P. J. Rayner, P. Norcott, K. M. Appleby, W. Iali, R. O. John, S. J. Hart, A. C. Whitwood and S. B. Duckett, Fine-tuning the efficiency of para-hydrogen-induced hyperpolarization by rational N-heterocyclic carbene design, *Nat. Commun.*, 2018, **9**, 4251.

114 R. W. Adams, S. B. Duckett, R. A. Green, D. C. Williamson and G. G. R. Green, A theoretical basis for spontaneous polarization transfer in non-hydrogenative parahydrogen-induced polarization, *J. Chem. Phys.*, 2009, **131**, 194505.

115 D. A. Barskiy, A. N. Pravdivtsev, K. L. Ivanov, K. V. Kovtunov and I. V. Koptyug, A simple analytical model for signal amplification by reversible exchange (SABRE) process, *Phys. Chem. Chem. Phys.*, 2016, **18**, 89–93.

116 S. Knecht and K. L. Ivanov, Quantitative quantum mechanical approach to SABRE hyperpolarization at high magnetic fields, *J. Chem. Phys.*, 2019, **150**, 124106.

117 S. Knecht, A. N. Pravdivtsev, J.-B. Hövener, A. V. Yurkovskaya and K. L. Ivanov, Quantitative description of the SABRE process: rigorous consideration of spin dynamics and chemical exchange, *RSC Adv.*, 2016, **6**, 24470–24477.

118 D. A. Barskiy, S. Knecht, A. V. Yurkovskaya and K. L. Ivanov, SABRE: Chemical kinetics and spin dynamics of the formation of hyperpolarization, *Prog. Nucl. Magn. Reson. Spectrosc.*, 2019, **114–115**, 33–70.

119 S. Knecht, D. A. Barskiy, G. Buntkowsky and K. L. Ivanov, Theoretical description of hyperpolarization formation in the SABRE-relay method, *J. Chem. Phys.*, 2020, **153**, 164106.

120 M. L. Truong, T. Theis, A. M. Coffey, R. V. Shchepin, K. W. Waddell, F. Shi, B. M. Goodson, W. S. Warren and E. Y. Chekmenev, 15N Hyperpolarization by Reversible Exchange Using SABRE-SHEATH, *J. Phys. Chem. C*, 2015, **119**, 8786–8797.

121 A. N. Pravdivtsev, A. V. Yurkovskaya, H.-M. Vieth, K. L. Ivanov and R. Kaptein, Level anti-crossings are a key factor for understanding para-hydrogen-induced hyperpolarization in SABRE experiments, *ChemPhysChem*, 2013, **14**, 3327–3331.

122 T. Theis, M. Truong, A. M. Coffey, E. Y. Chekmenev and W. S. Warren, LIGHT-SABRE enables efficient in-magnet catalytic hyperpolarization, *J. Magn. Reson.*, 2014, **248**, 23–26.

123 S. J. DeVience, R. L. Walsworth and M. S. Rosen, Preparation of nuclear spin singlet states using spin-lock induced crossing, *Phys. Rev. Lett.*, 2013, **111**, 173002.

124 S. Knecht, A. S. Kiryutin, A. V. Yurkovskaya and K. L. Ivanov, Efficient conversion of anti-phase spin order of protons into 15 N magnetisation using SLIC-SABRE, *Mol. Phys.*, 2019, **117**, 2762–2771.

125 A. N. Pravdivtsev, I. V. Skovpin, A. I. Svyatova, N. V. Chukanov, L. M. Kovtunova, V. I. Bukhtiyarov, E. Y. Chekmenev, K. V. Kovtunov, I. V. Koptyug and J.-B. Hövener, Chemical Exchange Reaction Effect on Polarization Transfer Efficiency in SLIC-SABRE, *J. Phys. Chem. A*, 2018, **122**, 9107–9114.

126 B. A. Rodin, J. Eills, R. Picazo-Frutos, K. F. Sheberstov, D. Budker and K. L. Ivanov, Constant-adiabaticity ultralow magnetic field manipulations of parahydrogen-induced polarization: application to an AA'X spin system, *Phys. Chem. Chem. Phys.*, 2021, **23**, 7125–7134.

127 B. A. Rodin, V. P. Kozinenko, A. S. Kiryutin, A. V. Yurkovskaya, J. Eills and K. L. Ivanov, Constant-

adiabaticity pulse schemes for manipulating singlet order in 3-spin systems with weak magnetic non-equivalence, *J. Magn. Reson.*, 2021, **327**, 106978.

128 T. Theis, P. Ganssle, G. Kervern, S. Knappe, J. Kitching, M. P. Ledbetter, D. Budker and A. Pines, Parahydrogen-enhanced zero-field nuclear magnetic resonance, *Nat. Phys.*, 2011, **7**, 571–575.

129 T. Theis, M. P. Ledbetter, G. Kervern, J. W. Blanchard, P. J. Ganssle, M. C. Butler, H. D. Shin, D. Budker and A. Pines, Zero-field NMR enhanced by parahydrogen in reversible exchange, *J. Am. Chem. Soc.*, 2012, **134**, 3987–3990.

130 M. C. Butler, G. Kervern, T. Theis, M. P. Ledbetter, P. J. Ganssle, J. W. Blanchard, D. Budker and A. Pines, Parahydrogen-induced polarization at zero magnetic field, *J. Chem. Phys.*, 2013, **138**, 234201.

131 D. B. Burueva, J. Eills, J. W. Blanchard, A. Garcon, R. Picazo-Frutos, K. V. Kovtunov, I. V. Koptyug and D. Budker, Chemical Reaction Monitoring using Zero-Field Nuclear Magnetic Resonance Enables Study of Heterogeneous Samples in Metal Containers, *Angew. Chem., Int. Ed.*, 2020, **59**, 17026–17032.

132 I. V. Zhukov, A. S. Kiryutin, F. Ferrage, G. Buntkowsky, A. V. Yurkovskaya and K. L. Ivanov, Total Correlation Spectroscopy across All NMR-Active Nuclei by Mixing at Zero Field, *J. Phys. Chem. Lett.*, 2020, **11**, 7291–7296.

133 D. A. Barskiy, M. C. D. Tayler, I. Marco-Rius, J. Kurhanewicz, D. B. Vigneron, S. Cikrikci, A. Aydogdu, M. Reh, A. N. Pravdivtsev, J.-B. Hövener, J. W. Blanchard, T. Wu, D. Budker and A. Pines, Zero-field nuclear magnetic resonance of chemically exchanging systems, *Nat. Commun.*, 2019, **10**, 3002.

134 J. W. Blanchard and D. Budker, in *eMagRes*, ed. R. K. Harris and R. L. Wasylishen, John Wiley & Sons, Ltd, Chichester, UK, 2007, pp. 1395–1410.

135 A. S. Kiryutin, A. V. Yurkovskaya and K. L. Ivanov, 15 N SABRE Hyperpolarization of Metronidazole at Natural Isotope Abundance, *ChemPhysChem*, 2021, **22**, 1470–1477.

136 J. Bernarding, G. Buntkowsky, S. Macholl, S. Hartwig, M. Burghoff and L. Trahms, J-coupling nuclear magnetic resonance spectroscopy of liquids in nT fields, *J. Am. Chem. Soc.*, 2006, **128**, 714–715.

137 B. A. Rodin, K. F. Sheberstov, A. S. Kiryutin, J. T. Hill-Cousins, L. J. Brown, R. C. D. Brown, B. Jamain, H. Zimmermann, R. Z. Sagdeev, A. V. Yurkovskaya and K. L. Ivanov, Constant-adiabaticity radiofrequency pulses for generating long-lived singlet spin states in NMR, *J. Chem. Phys.*, 2019, **150**, 64201.

138 S. Knecht, A. S. Kiryutin, A. V. Yurkovskaya and K. L. Ivanov, Mechanism of spontaneous polarization transfer in high-field SABRE experiments, *J. Magn. Reson.*, 2018, **287**, 74–81.

139 A. N. Pravdivtsev, K. L. Ivanov, A. V. Yurkovskaya, P. A. Petrov, H.-H. Limbach, R. Kaptein and H.-M. Vieth, Spin polarization transfer mechanisms of SABRE: A magnetic field dependent study, *J. Magn. Reson.*, 2015, **261**, 73–82.

140 K. F. Sheberstov, V. P. Kozinenko, A. S. Kiryutin, H.-M. Vieth, H. Zimmermann, K. L. Ivanov and A. V. Yurkovskaya, Hyperpolarization of cis-15 N2 -Azobenzene by Parahydrogen at Ultralow Magnetic Fields, *ChemPhysChem*, 2021, **22**, 1527–1534.

141 A. S. Kiryutin, A. V. Yurkovskaya, P. A. Petrov and K. L. Ivanov, Simultaneous 15 N polarization of several biocompatible substrates in ethanol-water mixtures by signal amplification by reversible exchange (SABRE) method, *Magn. Reson. Chem.*, 2021, **59**, 1216–1224.

142 A. S. Kiryutin, A. V. Yurkovskaya, H. Zimmermann, H.-M. Vieth and K. L. Ivanov, Complete magnetic field dependence of SABRE-derived polarization, *Magn. Reson. Chem.*, 2018, **56**, 651–662.

143 T. Theis, M. L. Truong, A. M. Coffey, R. V. Shchepin, K. W. Waddell, F. Shi, B. M. Goodson, W. S. Warren and E. Y. Chekmenev, Microtesla SABRE enables 10% nitrogen-15 nuclear spin polarization, *J. Am. Chem. Soc.*, 2015, **137**, 1404–1407.

144 S. B. Duckett and D. Blazina, The Study of Inorganic Systems by NMR Spectroscopy in Conjunction with Parahydrogen-Induced Polarisation, *Eur. J. Inorg. Chem.*, 2003, **2003**, 2901–2912.

145 S. B. Duckett and N. J. Wood, Parahydrogen-based NMR methods as a mechanistic probe in inorganic chemistry, *Coord. Chem. Rev.*, 2008, **252**, 2278–2291.

146 L. Buljubasich, M. B. Franzoni and K. Münnemann, in *Hyperpolarization Methods in NMR Spectroscopy*, ed. L. T. Kuhn, Springer Berlin Heidelberg, Berlin, Heidelberg, 2013, pp. 33–74.

147 J. Bargon, R. Giernoth, L. Greiner, L. T. Kuhn, S. Laue, A. Liese, H. G. Niessen, K. Woelk and J. Wöltinger, *In situ NMR methods in catalysis*, Springer, 2007.

148 S. Glöggler, J. Colell and S. Appelt, Parahydrogen perspectives in hyperpolarized NMR, *J. Magn. Reson.*, 2013, **235**, 130–142.

149 K. V. Kovtunov, I. E. Beck, V. I. Bukhtiyarov and I. V. Koptyug, Observation of Parahydrogen-Induced Polarization in Heterogeneous Hydrogenation on Supported Metal Catalysts, *Angew. Chem., Int. Ed.*, 2008, **47**, 1492–1495.

150 K. V. Kovtunov, V. V. Zhivonitko, A. Corma and I. V. Koptyug, Parahydrogen-induced polarization in heterogeneous hydrogenations catalyzed by an immobilized Au (III) complex, *J. Phys. Chem. Lett.*, 2010, **1**, 1705–1708.

151 V.-V. Telkki, V. V. Zhivonitko, S. Ahola, K. V. Kovtunov, J. Jokisaari and I. V. Koptyug, Microfluidic Gas-Flow Imaging Utilizing Parahydrogen-Induced Polarization and Remote-Detection NMR, *Angew. Chem., Int. Ed.*, 2010, **49**, 8363–8366.

152 Q. Gong, J. Klankermayer and B. Blümich, Organometallic Complexes in Supported Ionic-Liquid Phase (SILP) Catalysts: A PHIP NMR Spectroscopy Study, *Chem.–Eur. J.*, 2011, **17**, 13795–13799.

153 K. V. Kovtunov, V. V. Zhivonitko, I. V. Skovpin, D. A. Barskiy and I. V. Koptyug, in *Hyperpolarization Methods in NMR Spectroscopy*, Springer, 2012, pp. 123–180.

154 O. G. Salnikov, K. V. Kovtunov, D. A. Barskiy, V. I. Bukhtiyarov, R. Kaptein and I. V. Koptyug, Kinetic Study of Propylene Hydrogenation over Pt/Al2O3 by Parahydrogen-Induced Polarization, *Appl. Magn. Reson.*, 2013, **44**, 279–288.

155 K. V. Kovtunov, D. A. Barskiy, A. M. Coffey, M. L. Truong, O. G. Salnikov, A. K. Khudorozhkov, E. A. Inozemtseva, I. P. Prosvirin, V. I. Bukhtiyarov, K. W. Waddell, E. Y. Chekmenev and I. V. Koptyug, High-Resolution 3D Proton MRI of Hyperpolarized Gas Enabled by Parahydrogen and Rh/TiO_2 Heterogeneous Catalyst, *Chem.–Eur. J.*, 2014, **20**, 11636–11639.

156 K. V. Kovtunov, D. A. Barskiy, O. G. Salnikov, A. K. Khudorozhkov, V. I. Bukhtiyarov, I. P. Prosvirin and I. V. Koptyug, Parahydrogen-induced polarization (PHIP) in heterogeneous hydrogenation over bulk metals and metal oxides, *Chem. Commun.*, 2014, **50**, 875–878.

157 K. V. Kovtunov, M. L. Truong, D. A. Barskiy, I. V. Koptyug, A. M. Coffey, K. W. Waddell and E. Y. Chekmenev, Long-Lived Spin States for Low-Field Hyperpolarized Gas MRI, *Chem.–Eur. J.*, 2014, **20**, 14629–14632.

158 K. V. Kovtunov, M. L. Truong, D. A. Barskiy, O. G. Salnikov, V. I. Bukhtiyarov, A. M. Coffey, K. W. Waddell, I. V. Koptyug and E. Y. Chekmenev, Propane-d6 Heterogeneously Hyperpolarized by Parahydrogen, *J. Phys. Chem. C*, 2014, **118**, 28234–28243.

159 D. A. Barskiy, O. G. Salnikov, K. V. Kovtunov and I. V. Koptyug, NMR Signal Enhancement for Hyperpolarized Fluids Continuously Generated in Hydrogenation Reactions with Parahydrogen, *J. Phys. Chem. A*, 2015, **119**, 996–1006.

160 K. V. Kovtunov, O. G. Salnikov, V. V. Zhivonitko, I. V. Skovpin, V. I. Bukhtiyarov and I. V. Koptyug, Catalysis and Nuclear Magnetic Resonance Signal Enhancement with Parahydrogen, *Top. Catal.*, 2016, **59**, 1686–1699.

161 D. A. Barskiy, A. M. Coffey, P. Nikolaou, D. M. Mikhaylov, B. M. Goodson, R. T. Branca, G. J. Lu, M. G. Shapiro, V.-V. Telkki, V. V. Zhivonitko, I. V. Koptyug, O. G. Salnikov, K. V. Kovtunov, V. I. Bukhtiyarov, M. S. Rosen, M. J. Barlow, S. Safavi, I. P. Hall, L. Schröder and E. Y. Chekmenev, NMR Hyperpolarization Techniques of Gases, *Chem.–Eur. J.*, 2017, **23**, 725–751.

162 D. A. Barskiy, O. G. Salnikov, A. S. Romanov, M. A. Feldman, A. M. Coffey, K. V. Kovtunov, I. V. Koptyug and E. Y. Chekmenev, NMR Spin-Lock Induced Crossing (SLIC) dispersion and long-lived spin states of gaseous propane at low magnetic field (0.05 T), *J. Magn. Reson.*, 2017, **276**, 78–85.

163 D. B. Burueva, A. S. Romanov, O. G. Salnikov, V. V. Zhivonitko, Y.-W. Chen, D. A. Barskiy, E. Y. Chekmenev, D. W. Hwang, K. V. Kovtunov and I. V. Koptyug, Extending the lifetime of hyperpolarized propane gas through reversible dissolution, *J. Phys. Chem. C*, 2017, **121**, 4481–4487.

164 O. G. Salnikov, H.-J. Liu, A. Fedorov, D. B. Burueva, K. V. Kovtunov, C. Copéret and I. V. Koptyug, Pairwise hydrogen addition in the selective semihydrogenation of alkynes on silica-supported Cu catalysts, *Chem. Sci.*, 2017, **8**, 2426–2430.

165 D. B. Burueva, K. V. Kovtunov, A. V. Bukhtiyarov, D. A. Barskiy, I. P. Prosvirin, I. S. Mashkovsky, G. N. Baeva, V. I. Bukhtiyarov, A. Y. Stakheev and I. V. Koptyug, Selective Single-Site Pd− In Hydrogenation Catalyst for Production of Enhanced Magnetic Resonance Signals using Parahydrogen, *Chem.–Eur. J.*, 2018, **24**, 2547–2553.

166 O. G. Salnikov, K. V. Kovtunov, P. Nikolaou, L. M. Kovtunova, V. I. Bukhtiyarov, I. V. Koptyug and E. Y. Chekmenev, Heterogeneous Parahydrogen Pairwise Addition to Cyclopropane, *ChemPhysChem*, 2018, **19**, 2621.

167 N. M. Ariyasingha, O. G. Salnikov, K. V. Kovtunov, L. M. Kovtunova, V. I. Bukhtiyarov, B. M. Goodson, M. S. Rosen, I. V. Koptyug, J. G. Gelovani and E. Y. Chekmenev, Relaxation Dynamics of Nuclear Long-Lived Spin States in Propane and Propane-d 6 Hyperpolarized by Parahydrogen, *J. Phys. Chem. C*, 2019, **123**, 11734–11744.

168 O. G. Salnikov, P. Nikolaou, N. M. Ariyasingha, K. V. Kovtunov, I. V. Koptyug and E. Y. Chekmenev, Clinical-Scale Batch-Mode Production of Hyperpolarized Propane Gas for MRI, *Anal. Chem.*, 2019, **91**, 4741–4746.

169 D. B. Burueva, A. A. Smirnov, O. A. Bulavchenko, I. P. Prosvirin, E. Y. Gerasimov, V. A. Yakovlev, K. V. Kovtunov and I. V. Koptyug, Pairwise Parahydrogen Addition Over Molybdenum Carbide Catalysts, *Top. Catal.*, 2020, **63**, 2–11.

170 A. Svyatova, E. S. Kononenko, K. V. Kovtunov, D. Lebedev, E. Y. Gerasimov, A. V. Bukhtiyarov, I. P. Prosvirin, V. I. Bukhtiyarov, C. R. Müller and A. Fedorov, Spatially resolved NMR spectroscopy of heterogeneous gas phase hydrogenation of 1,3-butadiene with para hydrogen, *Catal. Sci. Technol.*, 2020, **10**, 99–104.

171 E. V. Pokochueva, D. B. Burueva, L. M. Kovtunova, A. V. Bukhtiyarov, A. Y. Gladky, K. V. Kovtunov, I. V. Koptyug and V. I. Bukhtiyarov, Mechanistic *in situ* investigation of heterogeneous hydrogenation over Rh/TiO2 catalysts: selectivity, pairwise route and catalyst nature, *Faraday Discuss.*, 2021, **229**, 161–175.

172 D. Burueva, A. Stakheev and I. Koptyug, Pd-based bimetallic catalysts for HET-PHIP, *Magn. Reson.*, 2021, **2**, 93–103.

173 D. A. Barskiy, K. V. Kovtunov, E. Y. Gerasimov, M. A. Phipps, O. G. Salnikov, A. M. Coffey, L. M. Kovtunova, I. P. Prosvirin, V. I. Bukhtiyarov and I. V. Koptyug, 2D mapping of NMR signal enhancement and relaxation for heterogeneously hyperpolarized propane gas, *J. Phys. Chem. C*, 2017, **121**, 10038–10046.

174 K. V. Kovtunov, I. V. Koptyug, M. Fekete, S. B. Duckett, T. Theis, B. Joalland and E. Y. Chekmenev,

Parahydrogen-Induced Hyperpolarization of Gases, *Angew. Chem., Int. Ed.*, 2020, **59**, 17788–17797.

175 J.-B. Hövener, A. N. Pravdivtsev, B. Kidd, C. R. Bowers, S. Glöggler, K. V. Kovtunov, M. Plaumann, R. Katz-Brull, K. Buckenmaier and A. Jerschow, Parahydrogen-based hyperpolarization for biomedicine, *Angew. Chem., Int. Ed.*, 2018, **57**, 11140–11162.

176 G. Buntkowsky, J. Bargon and H.-H. Limbach, A Dynamic Model of Reaction Pathway Effects on Parahydrogen-Induced Nuclear Spin Polarization, *J. Am. Chem. Soc.*, 1996, **118**, 8677–8683.

177 G. Buntkowsky, T. Gutmann, M. V. Petrova, K. L. Ivanov, U. Bommerich, M. Plaumann and J. Bernarding, Dipolar induced Para-Hydrogen-Induced Polarization, *Solid State Nucl. Magn. Reson.*, 2014, **63–64**, 20–29.

178 E. V. Pokochueva, D. B. Burueva, O. G. Salnikov and I. V. Koptyug, Heterogeneous Catalysis and Parahydrogen-Induced Polarization, *ChemPhysChem*, 2021, **22**, 1421–1440.

179 J. A. Aguilar, P. I. P. Elliott, J. López-Serrano, R. W. Adams and S. B. Duckett, Only para-hydrogen spectroscopy (OPSY), a technique for the selective observation of para-hydrogen enhanced NMR signals, *Chem. Commun.*, 2007, 1183–1185.

180 S. Knecht, S. Hadjiali, D. A. Barskiy, A. Pines, G. Sauer, A. S. Kiryutin, K. L. Ivanov, A. V. Yurkovskaya and G. Buntkowsky, Indirect Detection of Short-Lived Hydride Intermediates of Iridium N-Heterocyclic Carbene Complexes *via* Chemical Exchange Saturation Transfer Spectroscopy, *J. Phys. Chem. C*, 2019, **123**, 16288–16293.

181 N. V. Kireev, A. S. Kiryutin, A. A. Pavlov, A. V. Yurkovskaya, E. I. Musina, A. A. Karasik, E. S. Shubina, K. L. Ivanov and N. V. Belkova, Nickel(II) Dihydrogen and Hydride Complexes as the Intermediates of H_2 Heterolytic Splitting by Nickel Diazadiphosphacyclooctane Complexes, *Eur. J. Inorg. Chem.*, 2021, **2021**, 4265–4272.

182 M. E. Tadros and L. Vaska, para-Hydrogen conversion and hydrogen-deuterium equilibration catalyzed by diamagnetic iridium, platinum, and ruthenium complexes in nonaqueous solution (1), *J. Colloid Interface Sci.*, 1982, **85**, 389–410.

183 J. Matthes, S. Gründemann, G. Buntkowsky, B. Chaudret and H. H. Limbach, NMR Studies of the Reaction Path of the o-H_2/p-H_2 Spin Conversion Catalyzed by Vaska's Complex in the Solid State, *Appl. Magn. Reson.*, 2013, **44**, 247–265.

184 T. Pery, K. Pelzer, G. Buntkowsky, K. Philippot, H.-H. Limbach and B. Chaudret, Direct NMR evidence for the presence of mobile surface hydrides on ruthenium nanoparticles, *ChemPhysChem*, 2005, **6**, 605–607.

185 N. Rothermel, T. Röther, T. Ayvalı, L. M. Martínez-Prieto, K. Philippot, H.-H. Limbach, B. Chaudret, T. Gutmann and G. Buntkowsky, Reactions of D 2 with 1,4-Bis(diphenylphosphino) butane-Stabilized Metal Nanoparticles-A Combined Gas-phase NMR, GC-MS and Solid-state NMR Study, *ChemCatChem*, 2019, **11**, 1465–1471.

186 H.-H. Limbach, T. Pery, N. Rothermel, B. Chaudret, T. Gutmann and G. Buntkowsky, Gas phase 1H NMR studies and kinetic modeling of dihydrogen isotope equilibration catalyzed by Ru-nanoparticles under normal conditions: dissociative *vs.* associative exchange, *Phys. Chem. Chem. Phys.*, 2018, **20**, 10697–10712.

187 A. J. Rossini, A. Zagdoun, M. Lelli, A. Lesage, C. Copéret and L. Emsley, Dynamic nuclear polarization surface enhanced NMR spectroscopy, *Acc. Chem. Res.*, 2013, **46**, 1942–1951.

188 B. M. Goodson, Using injectable carriers of laser-polarized noble gases for enhancing NMR and MRI, *Concepts Magn. Reson.*, 1999, **11**, 203–223.

189 E. Brunner, Enhancement of surface and biological magnetic resonance using laser-polarized noble gases, *Concepts Magn. Reson.*, 1999, **11**, 313–335.

190 G. Sauer, D. Nasu, D. Tietze, T. Gutmann, S. Englert, O. Avrutina, H. Kolmar and G. Buntkowsky, Effective PHIP Labeling of Bioactive Peptides Boosts the Intensity of the NMR Signal, *Angew. Chem., Int. Ed.*, 2014, **53**, 12941–12945.

191 R. B. Merrifield, Solid phase peptide synthesis. I. The synthesis of a tetrapeptide, *J. Am. Chem. Soc.*, 1963, **85**, 2149–2154.

192 P. C. Soon, X. Xu, B. Zhang, F. Gruppi, J. W. Canary and A. Jerschow, Hyperpolarization of Amino Acid Precursors to Neurotransmitters with Parahydrogen Induced Polarization, *Chem. Commun.*, 2013, **49**, 5304–5306.

193 F. Gruppi, X. Xu, B. Zhang, J. A. Tang and A. Jerschow, Peptide Hydrogenation and Labeling with Parahydrogen, *Angew. Chem., Int. Ed.*, 2012, **51**, 11787–11790.

194 T. Trantzschel, M. Plaumann, J. Bernarding, D. Lego, T. Ratajczyk, S. Dillenberger, G. Buntkowsky, J. Bargon and U. Bommerich, Application of Parahydrogen-Induced Polarization to Unprotected Dehydroamino Carboxylic Acids, *Appl. Magn. Reson.*, 2013, **44**, 267–278.

195 D. Lego, M. Plaumann, T. Trantzschel, J. Bargon, H. Scheich, G. Buntkowsky, T. Gutmann, G. Sauer, J. Bernarding and U. Bommerich, Parahydrogen-induced polarization of carboxylic acids: a pilot study of valproic acid and related structures, *NMR Biomed.*, 2014, **27**, 810–816.

196 J. A. Tang, F. Gruppi, R. Fleysher, D. K. Sodickson, J. W. Canary and A. Jerschow, Extended para-hydrogenation monitored by NMR spectroscopy, *Chem. Commun.*, 2011, **47**, 958–960.

197 M. Koerner, G. Sauer, A. Heil, D. Nasu, M. Empting, D. Tietze, S. Voigt, H. Weidler, T. Gutmann, O. Avrutina, H. Kolmar, T. Ratajczyk and G. Buntkowsky, PHIP-label: parahydrogen-induced polarization in propargylglycine-containing synthetic oligopeptides, *Chem. Commun.*, 2013, **49**, 7839–7841.

198 M. L. J. Korsinczky, H. J. Schirra, K. J. Rosengren, J. West, B. A. Condie, L. Otvos, M. A. Anderson and D. J. Craik, Solution structures by 1H NMR of the novel cyclic trypsin inhibitor SFTI-1 from sunflower seeds and an acyclic permutant, *J. Mol. Biol.*, 2001, **311**, 579–591.

199 M. L. Korsinczky, H. J. Schirra and D. J. Craik, Sunflower trypsin inhibitor-1, *Curr. Protein Pept. Sci.*, 2004, **5**, 351–364.
200 S. J. de Veer, A. M. White and D. Craik, Sunflower Trypsin Inhibitor-1 (SFTI-1): Sowing Seeds in the Fields of Chemistry and Biology, *Angew. Chem., Int. Ed.*, 2020, **60**, 8050–8071.
201 S. Luckett, R. S. Garcia, J. J. Barker, A. V. Konarev, P. R. Shewry, A. R. Clarke and R. L. Brady, High-resolution structure of a potent, cyclic proteinase inhibitor from sunflower seeds, *J. Mol. Biol.*, 1999, **290**, 525–533.
202 H. Fittler, O. Avrutina, B. Glotzbach, M. Empting and H. Kolmar, Combinatorial tuning of peptidic drug candidates: high-affinity matriptase inhibitors through incremental structure-guided optimization, *Org. Biomol. Chem.*, 2013, **11**, 1848–1857.
203 H. Fittler, O. Avrutina, M. Empting and H. Kolmar, Potent inhibitors of human matriptase-1 based on the scaffold of sunflower trypsin inhibitor, *J. Pept. Sci.*, 2014, **20**, 415–420.
204 A. S. Kiryutin, G. Sauer, S. Hadjiali, A. V. Yurkovskaya, H. Breitzke and G. Buntkowsky, A highly versatile automatized setup for quantitative measurements of PHIP enhancements, *J. Magn. Reson.*, 2017, **285**, 26–36.
205 A. S. Kiryutin, G. Sauer, D. Tietze, M. Brodrecht, S. Knecht, A. V. Yurkovskaya, K. L. Ivanov, O. Avrutina, H. Kolmar and G. Buntkowsky, Ultrafast Single-Scan 2D NMR Spectroscopic Detection of a PHIP-Hyperpolarized Protease Inhibitor, *Chem.–Eur. J.*, 2019, **25**, 4025–4030.
206 A. Tal and L. Frydman, Single-scan multidimensional magnetic resonance, *Prog. Nucl. Magn. Reson. Spectrosc.*, 2010, **57**, 241–292.
207 P. Giraudeau and L. Frydman, Ultrafast 2D NMR: An Emerging Tool in Analytical Spectroscopy, *Annu. Rev. Anal. Chem.*, 2014, **7**, 129–161.
208 M. Gal and L. Frydman, Multidimensional NMR spectroscopy in a single scan, *Magn. Reson. Chem.*, 2015, **53**, 971–985.
209 B. Gouilleux, L. Rouger and P. Giraudeau, Ultrafast Multi-dimensional NMR: Principles and Recent Applications//Ultrafast Multi-dimensional NMR: Principles and Recent Applications, *eMagRes*, 2016, 913–922.
210 B. Gouilleux, L. Rouger and P. Giraudeau, Chapter Two - Ultrafast 2D NMR: Methods and Applications, *Annu. Rep. NMR Spectrosc.*, 2018, **93**, 75–144.
211 L. Frydman, T. Scherf and A. Lupulescu, The acquisition of multidimensional NMR spectra within a single scan, *Proc. Natl. Acad. Sci. U. S. A.*, 2002, **99**, 15858–15862.
212 L. Frydman and D. Blazina, Ultrafast two-dimensional nuclear magnetic resonance spectroscopy of hyperpolarized solutions, *Nat. Phys.*, 2007, **3**, 415.
213 A. N. Pravdivtsev, K. L. Ivanov, A. V. Yurkovskaya, H.-M. Vieth and R. Z. Sagdeev, New pulse sequence for robust filtering of hyperpolarized multiplet spin order, *Dokl. Phys. Chem.*, 2015, **465**, 267–269.
214 M. Fleckenstein, K. Herr, F. Theiß, S. Knecht, L. Wienands, M. Brodrecht, M. Reggelin and G. Buntkowsky, A disintegrin derivative as a case study for PHIP labeling of disulfide bridged biomolecules, *Sci. Rep.*, 2022, **12**, 2337.
215 S. Glöggler, R. Müller, J. Colell, M. Emondts, M. Dabrowski, B. Blümich and S. Appelt, Para-hydrogen induced polarization of amino acids, peptides and deuterium–hydrogen gas, *Phys. Chem. Chem. Phys.*, 2011, **13**, 13759–13764.
216 T. Ratajczyk, T. Gutmann, P. Bernatowicz, G. Buntkowsky, J. Frydel and B. Fedorczyk, NMR Signal Enhancement by Effective SABRE Labeling of Oligopeptides, *Chem.–Eur. J.*, 2015, **21**, 12616–12619.
217 T. Ratajczyk, G. Buntkowsky, T. Gutmann, B. Fedorczyk, A. Mames, M. Pietrzak, P. Szkudlarek and Z. Puzio, Magnetic Resonance Signal Amplification by Reversible Exchange of Selective PyFALGEA Oligopeptide Ligands Towards Epidermal Growth Factor Receptors, *ChemBioChem*, 2021, 855–860.
218 F. A. Gallagher, M. I. Kettunen, D.-E. Hu, P. R. Jensen, R. I. t. Zandt, M. Karlsson, A. Gisselsson, S. K. Nelson, T. H. Witney, S. E. Bohndiek, G. Hansson, T. Peitersen, M. H. Lerche and K. M. Brindle, Production of hyperpolarized 1,4-13C2malate from 1,4-13C2fumarate is a marker of cell necrosis and treatment response in tumors, *Proc. Natl. Acad. Sci. U. S. A.*, 2009, **106**, 19801–19806.
219 M. R. Clatworthy, M. I. Kettunen, D.-E. Hu, R. J. Mathews, T. H. Witney, B. W. C. Kennedy, S. E. Bohndiek, F. A. Gallagher, L. B. Jarvis, K. G. C. Smith and K. M. Brindle, Magnetic resonance imaging with hyperpolarized 1,4-(13)C2fumarate allows detection of early renal acute tubular necrosis, *Proc. Natl. Acad. Sci. U. S. A.*, 2012, **109**, 13374–13379.
220 L. Mignion, P. Dutta, G. V. Martinez, P. Foroutan, R. J. Gillies and B. F. Jordan, Monitoring chemotherapeutic response by hyperpolarized 13C-fumarate MRS and diffusion MRI, *Cancer Res.*, 2014, **74**, 686–694.
221 A. Eldirdiri, A. Clemmensen, S. Bowen, A. Kjaer and J. H. Ardenkjaer-Larsen, Simultaneous imaging of hyperpolarized 1,4-13 C2 fumarate, 1-13 Cpyruvate and 18 F-FDG in a rat model of necrosis in a clinical PET/MR scanner, *NMR Biomed.*, 2017, **30**, e3803.
222 B. Feuerecker, M. Durst, M. Michalik, G. Schneider, D. Saur, M. Menzel, M. Schwaiger and F. Schilling, Hyperpolarized 13C Diffusion MRS of Co-Polarized Pyruvate and Fumarate to Measure Lactate Export and Necrosis, *J. Cancer*, 2017, **8**, 3078–3085.
223 J. J. Miller, A. Z. Lau, P. M. Nielsen, G. McMullen-Klein, A. J. Lewis, N. R. Jespersen, V. Ball, F. A. Gallagher, C. A. Carr, C. Laustsen, H. E. Bøtker, D. J. Tyler and M. A. Schroeder, Hyperpolarized 1,4-13C2Fumarate Enables Magnetic Resonance-Based Imaging of Myocardial Necrosis, *JACC. Cardiovascular imaging*, 2018, **11**, 1594–1606.
224 E. Coleman, Z. Wang, M. He, E. Bier, J. Nouls, S. Womack, J. Mammarappallil, B. Driehuys and Y. T. Huang, Regional Gas Exchange Function Before and After Glycopyrrolate/

Formoterol Fumarate Measured by Hyperpolarized Xe-129 MRI in Chronic Obstructive Lung Disease, *Am. J. Respir. Crit. Care Med.*, 2019, **199**, A1122.

225 C. Laustsen, P. M. Nielsen, H. Qi, M. H. Løbner, J. Palmfeldt and L. B. Bertelsen, Hyperpolarized 1,4-13Cfumarate imaging detects microvascular complications and hypoxia mediated cell death in diabetic nephropathy, *Sci. Rep.*, 2020, **10**, 9650.

226 B. Ripka, J. Eills, H. Kouřilová, M. Leutzsch, M. H. Levitt and K. Münnemann, Hyperpolarized fumarate *via* parahydrogen, *Chem. Commun.*, 2018, **54**, 12246–12249.

227 J. Eills, E. Cavallari, C. Carrera, D. Budker, S. Aime and F. Reineri, Real-Time Nuclear Magnetic Resonance Detection of Fumarase Activity Using Parahydrogen-Hyperpolarized 1-13CFumarate, *J. Am. Chem. Soc.*, 2019, **141**, 20209–20214.

228 G. Pileio, S. Bowen, C. Laustsen, M. C. D. Tayler, J. T. Hill-Cousins, L. J. Brown, R. C. D. Brown, J. H. Ardenkjaer-Larsen and M. H. Levitt, Recycling and imaging of nuclear singlet hyperpolarization, *J. Am. Chem. Soc.*, 2013, **135**, 5084–5088.

229 G. Pileio, M. Carravetta and M. H. Levitt, Storage of nuclear magnetization as long-lived singlet order in low magnetic field, *Proc. Natl. Acad. Sci. U. S. A.*, 2010, **107**, 17135–17139.

230 A. S. Kiryutin, H. Zimmermann, A. V. Yurkovskaya, H.-M. Vieth and K. L. Ivanov, Long-lived spin states as a source of contrast in magnetic resonance spectroscopy and imaging, *J. Magn. Reson.*, 2015, **261**, 64–72.

231 D. Graafen, M. B. Franzoni, L. M. Schreiber, H. W. Spiess and K. Münnemann, Magnetic resonance imaging of (1)H long lived states derived from parahydrogen induced polarization in a clinical system, *J. Magn. Reson.*, 2016, **262**, 68–72.

232 J. Eills, J. W. Blanchard, T. Wu, C. Bengs, J. Hollenbach, D. Budker and M. H. Levitt, Polarization transfer *via* field sweeping in parahydrogen-enhanced nuclear magnetic resonance, *J. Chem. Phys.*, 2019, **150**, 174202.

233 M. H. Levitt, Long live the singlet state, *J. Magn. Reson.*, 2019, **306**, 69–74.

234 S. Mamone, N. Rezaei-Ghaleh, F. Opazo, C. Griesinger and S. Glöggler, Singlet-filtered NMR spectroscopy, *Sci. Adv.*, 2020, **6**, eaaz1955.

235 J. Matthes, T. Pery, S. Gründemann, G. Buntkowsky, S. Sabo-Etienne, B. Chaudret and H.-H. Limbach, Bridging the gap between homogeneous and heterogeneous catalysis: ortho/para H(2) conversion, hydrogen isotope scrambling, and hydrogenation of olefins by Ir(CO)Cl(PPh(3))(2), *J. Am. Chem. Soc.*, 2004, **126**, 8366–8367.

236 G. Buntkowsky, H.-H. Limbach, B. Walaszek, A. Adamczyk, Y. Xu, H. Breitzke, A. Schweitzer, T. Gutmann, M. Wächtler, N. Amadeu, D. Tietze and B. Chaudret, Mechanisms of Dipolar Ortho/Para-H_2O Conversion in Ice, *Z. Phys. Chem.*, 2008, **222**, 1049–1063.

237 J. Giberson, J. Scicluna, N. Legge and J. Longstaffe, Developments in benchtop NMR spectroscopy 2015–2020, *Annu. Rep. NMR Spectrosc.*, 2021, **102**, 153–246.

238 B. Blümich, Introduction to compact NMR: A review of methods, *TrAC, Trends Anal. Chem.*, 2016, **83**, 2–11.

239 M. E. Halse, Perspectives for hyperpolarisation in compact NMR, *TrAC, Trends Anal. Chem.*, 2016, **83**, 76–83.

240 P. M. Richardson, A. J. Parrott, O. Semenova, A. Nordon, S. B. Duckett and M. E. Halse, SABRE hyperpolarization enables high-sensitivity 1H and 13C benchtop NMR spectroscopy, *Analyst*, 2018, **143**, 3442–3450.

241 D. Gołowicz, K. Kazimierczuk, M. Urbańczyk and T. Ratajczyk, Monitoring Hydrogenation Reactions using Benchtop 2D NMR with Extraordinary Sensitivity and Spectral Resolution, *ChemistryOpen*, 2019, **8**, 196–200.

242 J. W. Blanchard, T. Wu, J. Eills, Y. Hu and D. Budker, Zero- to ultralow-field nuclear magnetic resonance J-spectroscopy with commercial atomic magnetometers, *J. Magn. Reson.*, 2020, **314**, 106723.

243 K. Buckenmaier, M. Rudolph, P. Fehling, T. Steffen, C. Back, R. Bernard, R. Pohmann, J. Bernarding, R. Kleiner, D. Koelle, M. Plaumann and K. Scheffler, Mutual benefit achieved by combining ultralow-field magnetic resonance and hyperpolarizing techniques, *Rev. Sci. Instrum.*, 2018, **89**, 125103.

244 S.-J. Lee, K. Jeong, J. H. Shim, H. J. Lee, S. Min, H. Chae, S. K. Namgoong and K. Kim, SQUID-based ultralow-field MRI of a hyperpolarized material using signal amplification by reversible exchange, *Sci. Rep.*, 2019, **9**, 12422.

245 N. Arunkumar, D. B. Bucher, M. J. Turner, P. TomHon, D. Glenn, S. Lehmkuhl, M. D. Lukin, H. Park, M. S. Rosen, T. Theis and R. L. Walsworth, Micron-Scale NV-NMR Spectroscopy with Signal Amplification by Reversible Exchange, *PRX Quantum*, 2021, **2**, 010305.